

GRAVITY ANALYSIS TO DETERMINE GEOMETRY OF SUPERPOSED LOW-ANGLE
DETACHMENT AND HIGH-ANGLE FAULTS IN THE WESTERN SILVER PEAK RANGE
AND NORTHERN FISH LAKE VALLEY, NEVADA

by

Melissa Kristin Ng



APPROVED BY SUPERVISORY COMMITTEE:

Carlos L. V. Aiken, Chair

Thomas H. Brikowski

Ignacio Pujana

Copyright 2018

Melissa Kristin Ng

All Rights Reserved

I would like to dedicate this thesis to my family.

FM5TAR

GRAVITY ANALYSIS TO DETERMINE GEOMETRY OF SUPERPOSED LOW-ANGLE
DETACHMENT AND HIGH-ANGLE FAULTS IN THE WESTERN SILVER PEAK RANGE
AND NORTHERN FISH LAKE VALLEY, NEVADA

by

MELISSA KRISTIN NG, BS

THESIS

Presented to the Faculty of
The University of Texas at Dallas
in Partial Fulfillment
of the Requirements
for the Degree of

MASTER OF SCIENCE IN
GEOSCIENCES

THE UNIVERSITY OF TEXAS AT DALLAS

December 2018

ACKNOWLEDGMENTS

I would like to thank my committee members, Dr. Carlos L. V. Aiken, Dr. Thomas Brikowski, and Dr. Ignacio Pujana, for their contributions, feedback, and flexibility during the duration of this work. Thank you to Dr. John S. Oldow for his mentorship and guidance while he was here. A special thanks to Dr. Carlos L. V. Aiken for taking over as my supervising professor when the time arose. I greatly appreciate all of my colleagues in the UT Dallas Geosciences Department, especially the members of the Ellison Miles Research group, all of whom contributed to the success of this project. I would like to thank my family and friends for their continued support through all the rough times during my thesis research. Thank you to my parents, Florence and Thomas Ng, for everything they have done for me to get me where I am today. A special thanks to Fred Treven for being my rock and continually supporting and encouraging me throughout my studies. Thank you to the Ellison Miles Foundation and Pioneer Natural Resources for their financial support.

October 2018

GRAVITY ANALYSIS TO DETERMINE GEOMETRY OF SUPERPOSED LOW-ANGLE
DETACHMENT AND HIGH-ANGLE FAULTS IN THE WESTERN SILVER PEAK RANGE
AND NORTHERN FISH LAKE VALLEY, NEVADA

Melissa Kristin Ng, MS
The University of Texas at Dallas, 2018

Supervising Professor: Carlos L. V. Aiken

Structures within the northern Eastern California shear zone (ECSZ) and central Walker Lane (CWL) are misaligned and have been kinematically linked since the mid-Miocene by a series of structural stepovers. Northwest directed extension within the stepover resulted in the formation of the Silver Peak - Lone Mountain (SPLM) extensional complex which transferred displacement via a shallowly northwest-dipping detachment. In the upper plate of the detachment, synextensional basins bounded by listric-normal faults accumulated deposits up to 2.5 km thick. The detachment was active from ~12 to 4 Ma, when displacement ceased and the kinematic mechanism of transfer changed from the detachment system to a curvilinear, high-angle fault system that cross-cut the detachment and upper-plate basins. To disentangle faults related to upper-plate basin formation and younger cross-cutting high-angle faults, we conducted a detailed gravity transect, spanning 26 km from exposures of the SPLM detachment in the Silver Peak Range, northwest across high-angle faults in the northern Fish Lake Valley. We collected 170 gravity measurements along the profile using a Scintrex CG-5 Autograv gravimeter with

positioning of 2.5 cm or better provided by two Leica Viva dual frequency GNSS receivers. Measurements were taken with a nominal spacing of 300 meters except over known high-angle faults, where the spacing was reduced to 50 meters for a distance of about 2 km, centered on the fault trace. The gravity data were terrain corrected and reduced to a datum density of 2.67 g/cm^3 to produce a complete Bouguer anomaly. Following removal of the regional field in calculation of a residual complete Bouguer anomaly, the data were modeled in 2D using Oasis Montaj GMSYS. Testing alternative geologic cross sections, we employed a 7 layer model, with densities ranging from 1.8 to 2.8 g/cm^3 . The modeling results indicate that eight down-to-the-west extensional faults mapped in the Silver Peak Range and northern Fish Lake Valley cross-cut both upper- and lower- plate rocks of the SPLM. These faults are related to the current episode of transtensional deformation which initiated $\sim 4 \text{ Ma}$, offset the detachment in a stair-step fashion with a cumulative vertical offset of 2.2 km, and currently help to transfer displacement from the northern ECSZ into the CWL.

TABLE OF CONTENTS

ACKNOWLEDGMENTS	v
ABSTRACT.....	vi
LIST OF FIGURES	ix
LIST OF TABLES	xi
CHAPTER 1 INTRODUCTION	1
CHAPTER 2 REGIONAL GEOLOGICAL FRAMEWORK	3
CHAPTER 3 STRUCTURE AND STRATIGRAPHY OF NORTHERN FISH LAKE VALLEY AND THE SILVER PEAK RANGE.....	7
3.1 Lithologic Units	8
3.2 Fault Geometry	16
3.3 Subsurface Morphology.....	21
CHAPTER 4 GEOPHYSICAL TRANSECT	29
4.1 Observed Gravity	29
4.2 Two-Dimensional Forward Models.....	36
4.3 Displacement Component Determinations	42
CHAPTER 5 DISCUSSIONS AND CONCLUSIONS	47
REFERENCES	49
BIOGRAPHICAL SKETCH	54
CURRICULUM VITAE	

LIST OF FIGURES

Figure 2.1 Physiographic map of the Silver Peak Range and surrounding areas, showing major fault traces, mountain ranges, and valley names. Location highlighted by the purple box on the California and Nevada state index map. The small white outline shows the extent of Figures 3.1, 3.2, and 4.4. The large white outline shows the extent of Figures 3.3 and 4.1. Major fault traces are shown in black and detachment faults are shown in yellow. Mountain ranges are labeled in black, valleys labeled in blue, and major fault systems in red. BSV - Big Smoky Valley, CSM - Columbus Salt Marsh, CV - Clayton Valley, DV - Death Valley, EPFZ - Emigrant Peak Fault Zone, EV - Eureka Valley, FCFS - Furnace Creek Fault System, FLV - Fish Lake Valley, FLVFZ - Fish Lake Valley Fault Zone, LM - Lone Mountain, LV - Lida Valley, OV - Owens Valley, PM - Palmetto Mountains, SPR - Silver Peak Range, WH- Weepah Hills, WM - White Mountains	5
Figure 3.1 Geologic map of the Silver Peak Range	9
Figure 3.2 Distribution of gravity stations along west-northwest gravity transect in the Silver Peak Range and VRS-1 well location. Location of Nevada Oil & Minerals geothermal well VRS-1 shown by green dot and interpreted stratigraphic section (left; after Garside and Schilling, 1979). Colors indicate formation; see legend in Figure 3.1. High-angle faults are shown in red and detachment faults are shown in blue.....	26
Figure 3.3 Residual complete Bouguer anomaly map of the Fish Lake Valley region. Figure only shows negative values to better illustrate the geometry of basins	28
Figure 4.1 Spatial distribution of gravity stations. Stations acquired by The University of Texas at Dallas from summer 2015 for this specific study are shown in pink, other stations taken by The University of Texas at Dallas from summers 2011-2016 are shown in blue, and stations obtained by the Pan American Center for Earth and Environmental Studies are shown in green	31
Figure 4.2 Complete Bouguer anomaly of the region. The black line from the SW Sierra Nevada to the NE central Great Basin was used to describe the characteristics of the regional trend. The black box shows the extent of Figures 3.3 and 4.1	33
Figure 4.3 First order polynomial of the complete Bouguer anomaly used as a regional trend ...	33
Figure 4.4 Residual complete Bouguer anomaly after removal of the regional trend of the Silver Peak Range.....	35
Figure 4.5 Two-dimensional representation of the residual complete Bouguer anomaly.....	35

- Figure 4.6 Two-dimensional geophysical merging model Modeled RCBA at field station locations shown by dotted line. Solid black line – forward calculated gravity; red line – error between observed residual and calculated gravity; triangle top – VRS-1 well. Geologic units are incorporated based on their mapped distribution in Figure 3.1. In this end-member model, high-angle faults are modeled to be listric, and merge into the planar low-angle detachment43
- Figure 4.7 Two-dimensional geophysical cross-cut model. Modeled RCBA at field station locations shown by dotted line. Solid black line – forward calculated gravity; red line – error between observed residual and calculated gravity; triangle top – VRS-1 well. Geologic units are incorporated based on their mapped distribution in Figure 3.1. In this end-member model, high-angle faults are modeled to cross-cut and offset the low-angle detachment in the subsurface44
- Figure 4.8 Fault displacement components. Block and trigonometric diagrams used in the derivation of fault displacement components. Components: D_{HC} – horizontal component of dip slip movement, SS – strike slip component, HE – horizontal extension, NS – net slip, V – vertical offset, D – dip slip component, Θ – true dip of the fault, \emptyset – acute angle between strike and inferred extension direction46

LIST OF TABLES

Table 4.1	Geologic units with brief lithologic descriptions and densities used in two-dimensional gravity models	37
-----------	--	----

CHAPTER 1

INTRODUCTION

Regions of large-magnitude extension characterized by a lower plate of metamorphic tectonites separated from a brittlely deformed upper-plate assemblage by a shallowly dipping detachment fault are well documented within the Basin and Range Province and constitute the classic metamorphic core complexes (Coney, 1979, 1980; Coney and Harms, 1984; Davis and Coney 1979). Several studies have documented that transcurrent stepovers can result in asymmetrical extensional complexes underlain by shallow detachment systems and may be common features in regions of transtensional deformation (Mancktelow and Pavlis, 1994; Oldow, 1992; Oldow et al., 1994; Oldow et al., 2003).

During the detachment process in large-magnitude extensional core complexes, upper-plate synextensional deposition in half-graben basins bounded by listric normal faults is typically observed. Most of these systems have experienced such great extension that the upper-plate assemblages are highly disarticulated and the relation between the synextensional deposits and coeval structures are lost (Oldow et al., 2009). The architecture of basins active during displacement and fragmentation of upper-plate assemblages can be pieced together using remnants of sedimentary and volcanic successions deposited during extension in order to make two-dimensional conceptual models of upper-plate morphology (Gans et al., 1989; Stewart and Diamond, 1990). Geometry of basins formed in low-magnitude extensional systems offers insight about the link between structures and basin growth, although extrapolation of these models to conditions found in systems of large-magnitude extension is largely speculative.

There is still a lack of understanding between the structural links of near-surface fault-controlled basins and how they relate to large-displacement detachment faults (Oldow et al., 2009).

In the Silver Peak-Lone Mountain extensional complex of west-central Nevada, the geometry of upper-plate synextensional fault bounded basins is well preserved. In the Silver Peak Range, there was an earlier history of synextensional deposition in basins bounded by listric faults that soled into a shallowly northwest-dipping detachment (Oldow et al., 2009). It has previously been speculated that at about 5-3 Ma, the region experienced a transition in kinematics, and deformation on the detachment apparently ceased preserving upper-plate basins (Henry and Perkins, 2001; Oldow et al., 2008; Walker et al., 2014). The area continued to experience deformation with the formation of a curvilinear array of high-angle faults. Surface mapping and borehole data do not reveal whether these curvilinear high-angle faults sole into the detachment or if they cross-cut the detachment and upper-plate basins.

Multiple generations of high-angle faulting within the Silver Peak Range make it difficult to distinguish between faults that controlled upper-plate basin formation, and faults that offset the basins based on surficial relationships. In the eastern Silver Peak Range, it is observed that some high-angle faults merge into the detachment and some high-angle faults offset the detachment, but further west there are no surface relations between the high-angle faults and the low-angle structure. This thesis addresses the subsurface geometries of the high-angle faults and the low-angle detachment and segregating post- and syn-detachment structures by using high-resolution gravity imaging. The main focus is on how the regional change in kinematics impacted the active high-angle faults in relation to the detachment and differentiating between faults that sole into and cross-cut the low angle structure.

CHAPTER 2

REGIONAL GEOLOGIC FRAMEWORK

The Eastern California shear zone and the central Walker Lane constitute a tectonic boundary zone accommodating differential motion between the northwest translating Sierra Nevada block and the west-northwest extending Basin and Range (Oldow, 2003). This tectonic boundary zone currently takes up to 20-25% of the relative motion between the Pacific and North American plates (Argus and Gordon, 1991; Thatcher et al., 1999; Bennett et al., 1999; Miller et al., 2001) and is dominated by simultaneous right lateral shear and extension (Hardyman and Oldow, 1991; Bennett et al., 2003), with active transtension being documented using Global Positioning System (GPS) velocities and earthquake focal mechanisms (Unruh et al., 2003). GPS velocities show a westward increase from 2-3 mm/year directed west-northwest in the central Great Basin to about 14 mm/year in the Sierra Nevada block (Dixon et al., 2000; Oldow et al., 2001; Oldow, 2003).

Structures within the northern Eastern California shear zone and central Walker Lane are misaligned and have been kinematically linked since the mid-Miocene by a series of structural stepovers (Oldow, 2003; Oldow et al., 2008, 2009). Northwest directed extension within the stepover resulted in the formation of the Silver Peak Range and the Weepah Hills –Lone Mountain Range which together form the Silver Peak-Lone Mountain extensional complex (Fig. 2.1). Active from the late Miocene to the Pliocene, the Silver Peak-Lone Mountain extensional complex transferred displacement east-northeast on the Furnace Creek fault system in the Eastern California shear zone onto a system of en echelon transcurrent faults of the central Walker Lane via a shallowly northwest dipping detachment that underlies the extensional

complex (Oldow et al., 1994, 2008). In the late Pliocene, the stepover experienced a kinematic reorganization with the onset of the current deformation field (Oldow et al., 2008) and the mechanism of transfer changed from a detachment system to a curvilinear fault system. Modern day displacement transfer from the northern Eastern California shear zone to the central Walker Lane is being accommodated primarily by east-northeast striking left oblique faults known as the Mina deflection (Fig. 2.1).

East of Fish Lake Valley, in the Silver Peak-Lone Mountain extensional complex (Fig. 2.1), a folded, shallowly dipping, northwest directed detachment system that exhumed metamorphic core complexes in west-northwest trending turtleback structures is exposed (Diamond and Ingersoll, 2002; Kirsch, 1971; Oldow, 1992; Oldow et al., 1994, 2003, 2009). Northwest-directed transport on the detachment created extensional and transcurrent faults which controlled deposition of Miocene to early Pliocene volcanic, volcanogenic, and sedimentary rocks in spatially restricted basins (Oldow et al., 2009). The low-angle detachment fault structurally separates an upper plate of Paleozoic rocks and Tertiary volcanics and sediments, constituted by the Oligocene-Miocene Icehouse Canyon assemblage, 12-6 Ma Coyote Hole Group, and the 4 Ma to present Fish Lake Valley assemblage, from a lower plate of metamorphic tectonites. North-northeast and west-northwest striking syndepositional faults soled into the underlying detachment and moved simultaneously to accommodate extension within the upper plate (Oldow et al., 2009). Displacement on the regional detachment eventually ceased due to the growth of turtleback structures produced by west-northwest-trending folds (Oldow et al., 1994, 2008, 2009).

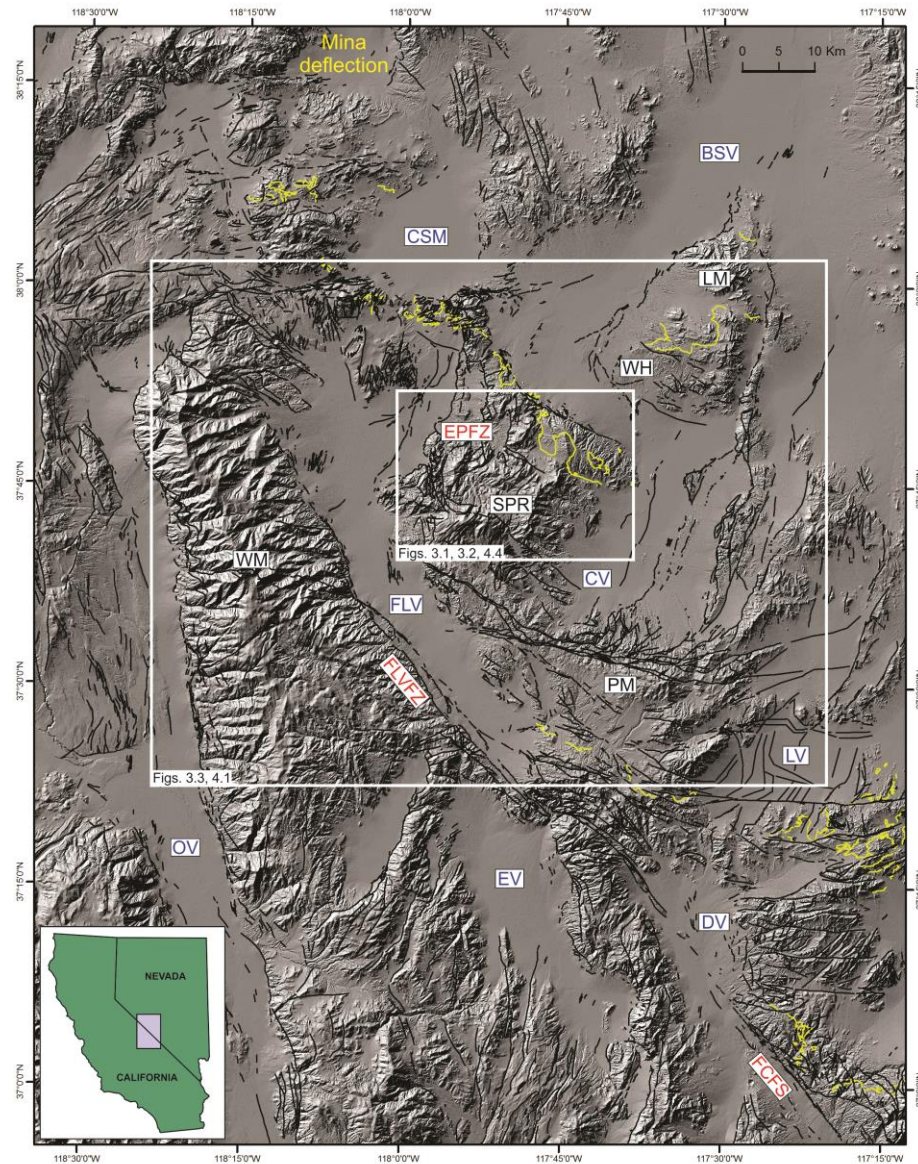


Figure 2.1. Physiographic map of the Silver Peak Range and surrounding areas, showing major fault traces, mountain ranges, and valley names. Location highlighted by the purple box on the California and Nevada state index map. The small white outline shows the extent of Figures 3.1, 3.2, and 4.4. The large white outline shows the extent of Figures 3.3 and 4.1. Major fault traces are shown in black and detachment faults are shown in yellow. Mountain ranges are labeled in black, valleys labeled in blue, and major fault systems in red. BSV - Big Smoky Valley, CSM - Columbus Salt Marsh, CV - Clayton Valley, DV - Death Valley, EPFZ - Emigrant Peak Fault Zone, EV - Eureka Valley, FCFS - Furnace Creek Fault System, FLV - Fish Lake Valley, FLVFZ - Fish Lake Valley Fault Zone, LM - Lone Mountain, LV - Lida Valley, OV - Owens Valley, PM - Palmetto Mountains, SPR - Silver Peak Range, WH- Weepah Hills, WM - White Mountains.

At about 5-3 Ma, the region saw a major change in kinematics with the initiation of the contemporary deformation field (Henry and Perkins, 2001; Oldow, 2003; Oldow et al., 2008; Stockli et al., 2003; Walker et al., 2014). Growth of west-northwest trending folds of the detachment system produced by the progressive deformation apparently locked the detachment and displacement transfer progressively stepped to the northwest (Petronis et al., 2009; Reheis and Sawyer, 1997; Oldow et al., 1994, 2008). In the late Pliocene to Quaternary, younger high-angle normal faults related to active displacement transfer cut across the western part of the Silver Peak Range and cut or locally reactivated older structures formed during earlier extension (Oldow et al., 2009).

CHAPTER 3

STRUCTURE AND STRATIGRAPHY OF NORTHERN FISH LAKE VALLEY AND THE SILVER PEAK RANGE

The Silver Peak Range is a dominant topographic feature located to the east of northern Fish Lake Valley and to the west of Clayton Valley (Fig. 2.1). The range stretches east-west for 40 km and north-south for about 30 km and exhibits a diamond shaped areal extent. In the Silver Peak Range, exposures of Cenozoic volcanic and sedimentary rocks occupy a region of high elevation bordered to the north and south by outcrops of pre-Cenozoic rocks (Oldow et al., 2009). The Cenozoic rocks are exposed in a 15 to 20 km wide belt that trends west-northwest across the central Silver Peak Range for about 30 km. From north to south, the Silver Peak Range rises from about 1900 m to 2800 m over a distance of 30 km and then decreases to over 1800 m over a distance of 25 km.

The Silver Peak Range is bounded by Clayton Valley and Fish Lake Valley on the east and west, respectively. To the north, the range is bounded by the Columbus Salt Marsh, and to the southeast, the range merges with the Palmetto Mountains (Fig. 2.1). To the east, Clayton Valley is a 20 km wide north-northeast trending basin that stretches north south for about 20 km. The valley floor is covered by Late Quaternary alluvium and ranges in elevation from 1300 m to a maximum of 1500 m in the east. The western margin of the Silver Peak Range is bounded by Fish Lake Valley, which extends north-south for about 70 km and is between 5-7 km wide in the south and broadens to about 20 km wide in the north. From south to north the basin elevation decreases from about 1580 m to 1470 m over a distance of 40 km. In the north, the basin bifurcates into western and eastern segments, and achieves elevations of about 1600 m and 1450

m, respectively. The northern boundary of the Silver Peak Range is truncated by east-northeast trending faults at the southern extent of the Columbus Salt Marsh. The Columbus Salt Marsh is a 15 by 15 km prismatic basin that ranges in elevation from 1380 m to 1450 m. At the southern extent, the Silver Peak Range merges with the west-northwest trending Palmetto Mountains. The mountain range is about 15 km wide and trends west-northwest for about 30 km and achieves a maximum elevation of 2800 m in the east.

3.1 Lithologic Units

In the Silver Peak Range metasedimentary pre-Cenozoic rocks and Cenozoic volcanic, sedimentary, and intrusive rocks are exposed (Fig. 3.1). Polydeformed greenschist to amphibolite facies metamorphic tectonites with Proterozoic protoliths are locally intruded by Cretaceous granitoids and are exposed in the Mineral ridge turtleback structure (Kirsch, 1971; Oldow et al., 1994; Oldow et al., 2003). Paleozoic siliciclastic and carbonate sedimentary rocks structurally overlie the metamorphic tectonites and depositionally underlie the Cenozoic stratigraphy. Unconformably overlying the pre-Cenozoic rocks are three major unconformably-bounded Cenozoic volcanic-sedimentary sequences ranging from the late Oligocene to early Miocene, mid to late Miocene, and Pliocene to Pleistocene.

The lithology exposed in the Silver Peak Range is subdivided into an upper- and lower-plate assemblage that is structurally separated by a shallow northwest-dipping detachment. The Silver Peak Range exposes an upper-plate assemblage consisting of upper Proterozoic and lower Paleozoic carbonates and clastics unconformably overlain by late Cenozoic volcanic and sedimentary successions. The lower-plate assemblage underlies the detachment and is composed

of deformed upper Proterozoic metasedimentary rocks intruded by several generations of Mesozoic plutons.

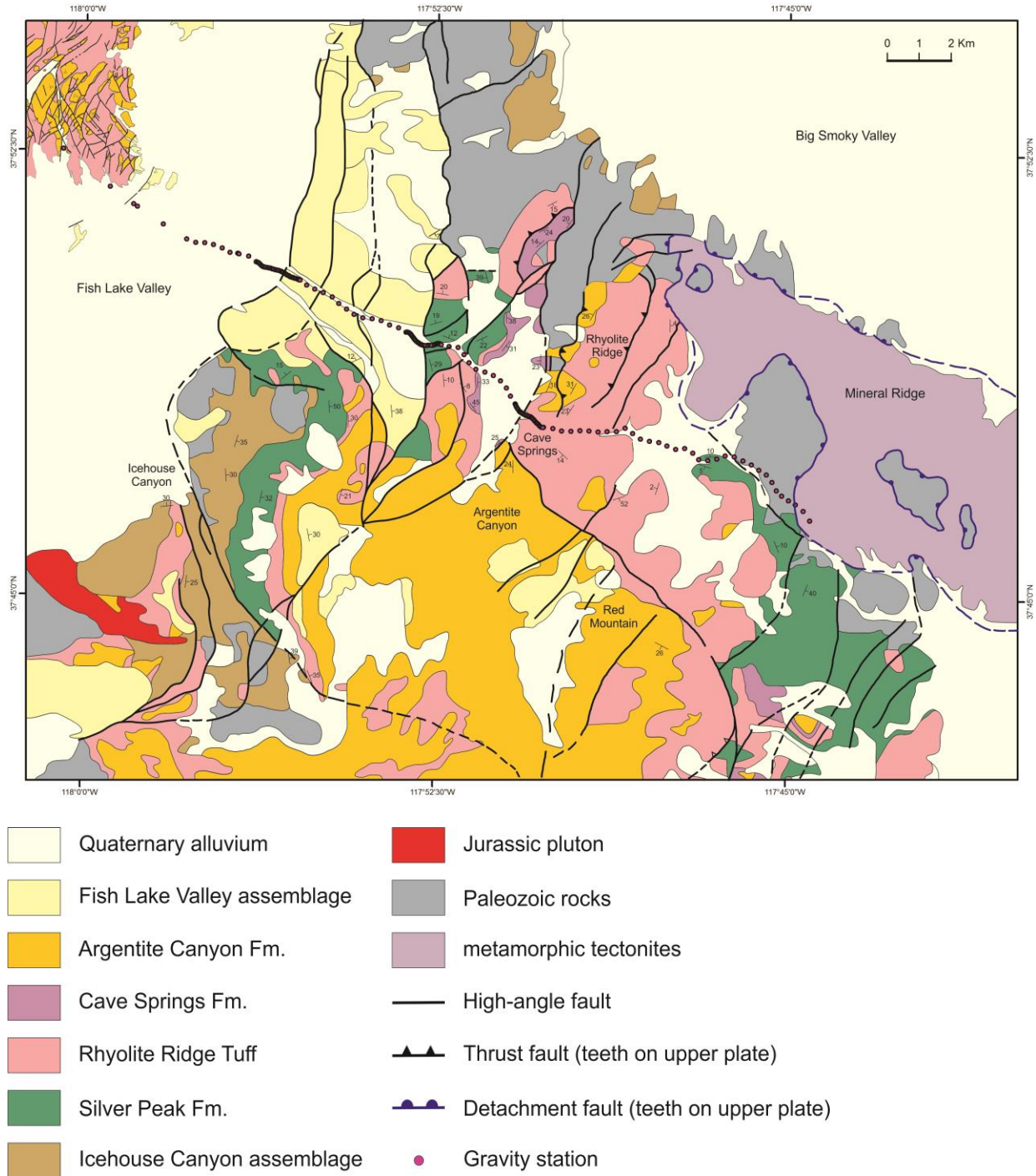


Figure 3.1. Geologic map of the Silver Peak Range. Adapted from Oldow et al., 2009.

Upper-plate Assemblage

In the Silver Peak Range, the upper-plate assemblage is composed of weakly metamorphosed Paleozoic siliciclastic and carbonate sedimentary rocks overlain by Cenozoic volcanic and sedimentary successions (Fig. 3.1). The pre-Cenozoic rocks of the upper-plate succession consist of weakly metamorphosed greenschist facies upper Proterozoic and lower Paleozoic carbonates and clastics. The Proterozoic to lower Paleozoic rocks are disarticulated remnants of the miogeosynclinal succession of the western United States (Albers and Stewart, 1972; Stewart and Poole, 1974; Oldow et al., 1989) that records the history of continental break-up and development of a passive margin that initiated in the early pre-Cambrian. Fault bound slices of upper Proterozoic carbonate and clastic rocks of Deep Springs and Campito Formations are preserved in the upper-plate together with Cambrian and Ordovician fossiliferous carbonate, argillite, and sandstone of the Poleta, Harkless, Mule Spring, and Emigrant Formations (Albers and Stewart, 1972; Oldow et al., 2003). Exposures of lower Paleozoic argillite, chert, and resedimented carbonate rocks of the Palmetto Formation are in thrust contact with the lower Cambrian rocks of the Harkless, Mule Spring, Poleta, and Campito Formations (Albers and Stewart, 1972; Oldow, 1984). The Ordovician Palmetto Formation rocks constitute the upper plate of the Roberts Mountains thrust system, which was emplaced during deformation in the mid-Paleozoic (Oldow, 1984). Regional burial metamorphism took place after this time. The lower Paleozoic miogeosynclinal succession and underlying Proterozoic rocks are composed of interbedded limestone, argillite, dolomite, and quartzite and have an aggregate stratigraphic thickness of more than 15 km (Albers and Stewart, 1972).

In the upper-plate assemblage, the Cenozoic stratigraphy records a complex history of volcanism and synorogenic deposition dominated by interleaved volcanic and volcanogenic rocks (Oldow et al., 2009). The Cenozoic section rests unconformably on Pre-Cenozoic upper-plate rocks and consists of three major volcanic-sedimentary successions named here in ascending stratigraphic order: Icehouse Canyon assemblage, Coyote Hole Group, and the Fish Lake Valley assemblage (Fig. 3.1). Many of the units are lithologically heterogeneous and show variations in age, composition, and thickness of constituent rocks. The Icehouse Canyon assemblage is a heterogeneous succession of clastic and volcanic rocks spatially restricted to a belt of west-northwest trending basins that were deposited prior to large-magnitude extension, and have an arc magmatism affinity (Kerstetter et al., 2016). The Coyote Hole Group consists of several unconformably bounded sequences that, in ascending order, constitute the Silver Peak Formation, the Rhyolite Ridge tuff, Cave Springs Formation, and the Argentite Canyon Formation, constituting a bi-modal extensional volcanic sequence. The Fish Lake Valley assemblage unconformably overlies units of the Coyote Hole Group and consists of a succession of poorly lithified clastic rocks interleaved with basalt flows, representing the termination of local volcanism.

Icehouse Canyon Assemblage. The Icehouse Canyon assemblage consists of a basal conglomerate containing clasts derived from lower Paleozoic lithologies, a middle welded to nonwelded rhyolite tuff member, and an upper unit composed of andesite lava, lahar, and debris flows (Robinson et al., 1968, 1976; Oldow et al., 2009). Unit thickness varies and reaches up to 500 m thick in the west-central part of the range to zero m ~5 km to the south and 12 km to the north (Fig. 3.1). Rhyolitic rocks within the succession are dated by K-Ar as 21.5-22.8 Ma and

correlate to a succession of ash-flow tuffs that form the basal part of the Cenozoic section (Robinson et al., 1968). The Icehouse canyon assemblage rests directly on Paleozoic rocks.

Coyote Hole Group. The Coyote Hole Group is a late Tertiary volcanogenic-volcanic succession overlying the Icehouse Canyon assemblage that provides a depositional record of the progressive deformation associated with upper-plate transport and disarticulation within the Silver Peak Range during large-magnitude extension. Rocks within this synorogenic sequence accumulated within rectilinear and discontinuous basins bounded by west-northwest and north-northeast striking faults during extension and exhumation of metamorphic core complexes (Oldow et al., 2009). The Coyote Hole Group succession rest on various units of the extensional complex exposed in the Silver Peak Range. In the eastern Silver Peak Range, Coyote Hole Group rocks structurally overlie metamorphic tectonites of the lower-plate assemblage exposed on Mineral Ridge (Fig. 3.1). In the western part of the range, rocks of the Coyote Hole Group rest with angular unconformity on differing units of the upper-plate assemblage and display variations in thickness and lateral distribution across the range. Virtually all units are found in depositional contact with older rocks and significant differences in the stratigraphy from area to area is a result of local omission of internal units.

Silver Peak Formation. The Silver Peak Formation is composed of a sedimentary succession consisting of interbedded shale, sandstone, and conglomerate containing components of Tertiary volcanic and Paleozoic detritus. Unit thickness varies from 5 m to 2000 m due to deposition in fault-bounded basins formed during extension. Ash-flow tuffs interbedded with the sedimentary rocks were dated with K-Ar as 13-11 Ma (Evernden et al., 1964; Evernden and James, 1964; Stewart and Diamond, 1990). The Silver Peak Formation rests depositionally on

both the Icehouse Canyon assemblage and Paleozoic rocks and in some places is found in structural contact with the lower-plate metamorphic tectonites (Fig. 3.1).

Rhyolite Ridge Tuff. The Rhyolite Ridge tuff is composed of quartz-feldspar lithic tuff containing minor biotite, phenocrystic-rich lithic tuff, and massive lithic tuff breccia. Locally, the unit is interbedded with rhyolitic lava flows composed of flow-banded aphanitic rhyolite that weathers pink to gray (Oldow et al., 2009). Unit reaches thicknesses of up to 425 m but is typically much thinner and exhibits lateral pinch outs where the rocks can range from zero to 300 m over a distance of less than a kilometer. The age of the tuff was determined in several areas of the central Silver Peak Range (by $^{40}\text{Ar}/^{39}\text{Ar}$ dating). Biotite separated from a sample collected at the base of the Rhyolite Ridge Tuff in the Cave Springs Canyon drainage (Fig. 3.1) has a $^{40}\text{Ar}/^{39}\text{Ar}$ age of 6.9 ± 0.9 Ma and a $^{40}\text{Ar}/^{39}\text{Ar}$ age on sanidine of 6.02 ± 0.03 Ma (Oldow et al., 2009). A sample taken from the eastern flank of Rhyolite Ridge, beneath the upper contact of the tuff with overlying Argentite Canyon Formation (Fig. 3.1), provided a $^{40}\text{Ar}/^{39}\text{Ar}$ age on sanidine of 6.03 ± 0.03 Ma. Another sample was collected ~120 m below the contact with the overlying Argentite Canyon Formation and yielded a $^{40}\text{Ar}/^{39}\text{Ar}$ age of 6.09 ± 0.03 Ma on sanidine (Oldow et al., 2009). The Rhyolite Ridge tuff typically overlies the Silver Peak Formation, but in some areas, it rests directly on the Icehouse Canyon assemblage or the Paleozoic rocks (Fig. 3.1).

Cave Springs Formation. The Cave Spring Formation is best exposed in the west-central Silver Peak Range (Fig. 3.1) and consists of basal travertine deposits, interbedded volcanogenic argillite, sandstone, and conglomerate. Unit reaches a maximum thickness of 300 m, but it is typically thinner, and ranges from 5 m to 100 m (Oldow et al., 2009). The Cave Springs

Formation is typically found in depositional contact with the underlying Rhyolite Ridge Tuff, but due to erosion, it is also found overlying the Silver Peak Formation in several locales (Fig. 3.1).

Argentite Canyon Formation. The Argentite Canyon Formation is the youngest member of the Coyote Hole Group and it consists of thick succession of feldspar porphyry flows, latite ashflow tuff and subordinate interleaved tuff breccias. This unit ranges in thickness from 30 m to in excess of 850 m throughout the Silver Peak Range. K-Ar ages of 5.9 and 6.1 Ma were reported on two of the flows exposed along the southern margin of Cenozoic outcrops by Robinson et al. (1976). A sample from the base of the Argentite Canyon Formation taken from the northern flank of Rhyolite Ridge (Fig. 3.1) was dated by $^{40}\text{Ar}/^{39}\text{Ar}$ and yielded an age on sanidine of 5.87 ± 0.02 Ma. Along the western range, a sample was taken from the top of the unit, just below the contact of the overlying Fish Lake Valley assemblage, and provided a $^{40}\text{Ar}/^{39}\text{Ar}$ age on sanidine of 5.85 ± 0.03 Ma (Oldow et al., 2009). Unit rests depositionally on the Cave Springs Formation, the Rhyolite Ridge Tuff, and locally on Paleozoic rocks. In several locations, it depositionally overlies and caps high-angle faults that controlled depositional pattern of older units of the Coyote Hole Group (Oldow et al., 2009).

Fish Lake Valley Assemblage. Rocks of the Coyote Hole Group are overlain unconformably by poorly lithified clastic rocks of the Fish Lake Valley assemblage. This unit is composed of poorly lithified claystone with interbeds of siltstone and sandstone, intercalated pebble to boulder conglomerate, sandstone, and argillite, and is locally underlain and interleaved with basalt flows. Unit reaches a thickness of 550 m in higher parts of the range (Oldow et al., 2009). Robinson et al., (1968) reported a whole-rock K-Ar age of 4.8 Ma on basalt flows and farther west along the northern margin of Fish Lake Valley, Lee et al., (2003) provided an age of

3.0 Ma by (U-Th)/He thermochronology on apatite. Near the western flank of the central Silver Peak Range (Fig. 3.1), basalt flows exposed near the base of the section were dated, and provided whole-rock $^{40}\text{Ar}/^{39}\text{Ar}$ ages of 3.71 ± 0.01 Ma and 3.76 ± 0.04 Ma (Oldow et al., 2009). The Fish Lake Valley assemblage locally overlies units of the Coyote Hole Group unconformably.

Lower-plate Assemblage

The lower-plate assemblage exposed on Mineral Ridge (Fig. 3.1) is composed of ductilely deformed upper Proterozoic metasedimentary rocks and several generation of igneous intrusive rocks that record a history of progressive deformation (Oldow et al., 2003). During late Cretaceous deformation and regional metamorphism, primary contact relationships shared by metasedimentary rocks were structurally transposed and true stratigraphic thicknesses are not known. Upper Proterozoic rocks consist of pelitic schist and dolomitic marble of the Wyman formation that pass upward into dolomitic marble and dolomite of the Reed formation (Albers and Stewart, 1972). Although the basal contact of the Wyman Formation is not observed, Albers and Stewart (1972) report a thickness of 400 m for the Wyman and a thickness of 500 m for the Reed dolomite. These Precambrian rocks were intruded by Mesozoic granitoids and were complexly folded and metamorphosed in pre-Tertiary time. The oldest intrusive rocks within the lower-plate assemblage are late Cretaceous in age and consist of medium-grained leucogranite and quartz monzonite (Oldow et al., 2003).

3.2 Fault Geometry

The key question in this study is the structural role of high-angle faults in the Silver Peak Range and northern Fish Lake Valley. Do the high-angle structures merge with or cross-cut the low-angle detachment? In the Silver Peak Range, a network of north-northeast and west-northwest striking faults formed prismatic fault blocks composed of Cenozoic and pre-Cenozoic rocks (Fig. 3.1; Oldow et al., 2009). The two sets of high-angle faults are closely associated with the geometry and distribution of synextensional stratigraphic units. North-northeast striking faults are locally linked by west-northwest trending fault segments and terminate to the north and south into the west-northwest trending structures. In the eastern part of the Silver Peak Range, a low-angle detachment fault is exposed and structural contacts between the upper- and lower-plates can be observed. In this area, high-angle faults are observed to both merge into and cross-cut the Mineral Ridge detachment (Fig. 3.1). In the western Silver Peak Range, high-angle faults show no surface relationships with the eastern detachment, which can make it difficult to determine how these faults interact with the detachment in the subsurface.

Throughout the Silver Peak Range, north-northeast trending high-angle faults are observed to both merge into and cross-cut west-northwest trending structures. In the southeastern Silver Peak Range, a system of north-northeast striking faults displaying evidence of displacement during deposition of the Coyote Hole Group is preserved (Fig. 3.1). This network of north-northeast trending structures, south of Mineral Ridge (Fig. 3.1), display a down-to-the-west sense and cut rocks of the Silver Peak Formation. The normal faults can be traced to the north where they merge with the underlying detachment fault and traced to the south where they intersect with a west-northwest trending structure. To the southwest of the

west-northwest longitudinal fault near Red Mountain (Fig. 3.1), there is a 4 km wide zone of northeasterly striking faults. These faults juxtapose rocks of the Rhyolite Ridge tuff, Argentite Canyon Formation, and Fish Lake Valley assemblages. Along strike to the north, this system of structures are truncated by a west-northwest trending fault. To the south, some structures are traced until they are truncated by the southernmost west-northwest trending fault, but some structures are more difficult to locate due to poor exposure. To the west of the Mineral Ridge turtleback, the western flank of Rhyolite Ridge is underlain by a west-directed thrust fault (Fig. 3.1). This thrust fault uplifts Rhyolite Ridge tuff and Argentite Canyon Formation in the hanging wall to the west over a footwall consisting of Argentite Canyon Formation rocks resting unconformably on Paleozoic rocks. Fault displacement decreases along strike, and the fault trace disappears to the south along the base of Rhyolite Ridge (Oldow et al., 2009). Several hundred meters to the east of this fault, there is a north-northeast striking, east directed thrust fault that marks the eastern boundary of Rhyolite Ridge. This fault carries units of the Rhyolite Ridge tuff in the western hanging wall over coeval footwall units to the east. Along strike to the north, the fault swings to the northwest and merges with a west-northwest striking fault. This west-northwest striking fault dips steeply to the south and juxtaposes Rhyolite Ridge tuff rocks in the southern footwall with Paleozoic rocks in the hanging wall. This fault can be traced for about 2 km to the northwest, where it is buried beneath a depositional contact with the Argentite Canyon Formation. About 600 m northwest of this fault a pair of north-northeast to east-northeast trending faults are observed. The faults dip northwesterly and juxtapose Rhyolite Ridge tuff, Paleozoic, and metamorphic rocks. Traced along strike towards the east, the pair of structures is observed to cross-cut and offset the low-angle structure and metamorphic tectonites. A few

hundred meters to the east of the east directed thrust there is a north-northeast trending normal fault with a down-to-the-west sense. Rocks of the Rhyolite Ridge tuff are exposed on both sides of the fault, and along strike ~4 km to the north, the fault is truncated by and does not cross-cut the detachment. Along the western Silver Peak Range, a curvilinear system of north-striking high-angle faults divides the upper-plate assemblage into several structural panels (Oldow et al., 2009). This network of faults are a part of the Emigrant Peak fault zone and form a system of splays that exhibit down-to-the-west displacement stretching from the western range front to the western flank of the topographic axis of the range. The complex anastomosing pattern of faults ramify towards the northeast and to the south, they merge and cut across a west-northwest trending structure. The westernmost range front fault forms a scarp in alluvium up to ~30 m high and juxtaposes rocks of the Fish Lake Valley assemblage with alluvial deposits in the playa. The eastern boundary of this fault zone is marked by a north-striking fault that exposes Paleozoic and Cenozoic rocks in the footwall. Within the eastern and western bounding structures, exposures of the Fish Lake Valley assemblage form a broad belt of subdued topography stretching along the western range front. The southern boundary of this low relief area is marked by a west-northwest trending fault with a down-to-the-west sense. This network of structures merge to the south and are deflected to the southwest, where they ultimately pass into the range-front fault system (Oldow et al., 2009).

In the Silver Peak Range, west-northwest striking longitudinal faults have acted as transfer zones, accommodating differential extension in basins linked by displacement transfer structures (Faulds and Varga, 1998). The west-northwest trending faults are well exposed along the southern margin of Cenozoic exposures and along the central axis of the range (Fig. 3.1).

The faults have continuous traces up to 12 km, spanning the width of the range, but the lateral continuity of the structures across the western margin of the range is obstructed by younger northerly striking faults. In the southwestern Silver Peak Range, near Icehouse Canyon (Fig. 3.1), a west-northwest trending fault marks the southern extent of Coyote Hole Group rocks. In the west, the fault is well located where it juxtaposes Paleozoic and Cenozoic rocks. It can be traced towards the southeast for ~ 5 km where it is cut by a northeasterly striking system of normal faults with a down-to-the-west sense. East of the northerly striking faults, the structure is located with more difficulty where Icehouse Canyon assemblage rocks are exposed on both sides of the fault. South of the fault trace, Coyote Hole Group units are thin, nearly flat lying, and rest on Paleozoic or Icehouse Canyon assemblage rocks. To the north, Coyote Hole Group rocks exhibit substantial differences in thickness and tilt across north-northeast striking faults that do not cut the transfer fault. Along the west-northwest trending central axis of the belt of Cenozoic rocks in the Silver Peak Range, another longitudinal fault is exposed. To the east of Red Mountain (Fig. 3.1), the fault is well preserved and observed to truncate high-angle faults, but to the west of Cave Springs (Fig. 3.1), the fault is disrupted by a network of northeast trending faults that cut it at a high-angle. This fault juxtaposes thick accumulations of Rhyolite Ridge Tuff to the north with Argentite Canyon Formation rocks in the south. To the south, Argentite Canyon Formation rocks reach a thickness in excess of 850 m, whereas to the north the same unit only reaches a maximum thickness of 30 m. Over 550 m of Fish Lake Valley assemblage rests on Argentite Canyon Formation in the south, and in the north, rocks of the same unit are only exposed along the western range front. East of Red Mountain, the west-northwest trending fault curves to the southwest and merges with a north-northeast striking thrust fault with top-to-the-

southeast displacement (Fig. 3.1). Near the western part of the range, there is a west-northwest fault that juxtaposes a thick accumulation of Coyote Hole Group rocks resting on Icehouse Canyon assemblage and Paleozoic rocks in the south against rocks of the Fish Lake Valley assemblage to the north. The fault lies along the western projection, and could be a reactivated segment of the central longitudinal fault system (Oldow et al., 2009).

A low-angle detachment fault that juxtaposes upper- and lower- plate units of contrasting age, lithology, and structure is exposed in the eastern Silver Peak Range on Mineral Ridge (Fig. 3.1). The Mineral Ridge detachment fault is an undulatory, elongate, dome-shaped fault surface, whose long axis trends approximately N60-70W (Kirsch, 1971), and whose form controls the physiography of mineral ridge (Diamond and Ingersoll, 2002). The Mineral Ridge detachment exposed in the turtleback structure was active in the mid-Miocene to Pliocene and served as a decoupling surface that the west-northwest and north-northeast striking faults soled into (Oldow et al., 1994; 2009). Extension on the shallowly dipping detachment juxtaposed an upper-plate assemblage of Paleozoic metasedimentary rocks and Cenozoic volcanics with a lower-plate composed of amphibolite-facies metamorphic tectonites and Cenozoic intrusive rocks (Oldow et al., 1994). Movement on the detachment initiated by 12 Ma and ceased by 3 to 5 Ma as indicated by exhumation ages of the footwall and age of synextensional rocks within north-northeast trending basins that formed in the hanging wall during movement on the detachment (Oldow et al., 1994). The detachment fault and overlying upper-plate rocks are warped in broad northwest trending folds with doubly plunging axes. The folds have wavelengths of ~ 15 km, define the long axis of the turtlebacks, and are parallel to the direction of upper-plate transport (Oldow et al., 1994). West-northwest folding of the Mineral Ridge detachment into doubly-

plunging anticlines reflect localized shortening within the Silver Peak-Lone Mountain extensional stepover and were accompanied by 20° to 30° of paleomagnetically determined clockwise rotation (Oldow et al., 2008; Petronis et al., 2002; 2007).

In the eastern part of the Silver Peak Range (Fig. 3.1), Paleozoic and Cenozoic rocks of the upper-plate assemblage are in structural contact with the underlying metamorphic tectonites of the lower plate. In this region, both high-angle faults and the low-angle detachment are exposed and surface relations are observed. Along the northwest flank of mineral ridge, a pair of curvilinear high-angle faults dipping down to the north is present. These two faults trend north-northeast for about one km before changing orientation to trend east-northeast, where they are seen to cut and offset the detachment about 300 m. A few kilometers south of the two curvilinear high-angle faults that cut the detachment, on the eastern flank of Rhyolite Ridge, a north-northeast trending high-angle fault with down-to-the-west displacement is exposed. This fault can be traced for about 4 km to northeast where it intersects and merges into the low-angle detachment. In the eastern area of the Silver Peak Range, high-angle faults are observed to both cross-cut the detachment as well as intersect and be terminated by the low-angle detachment. In the western Silver Peak Range, high-angle faults do not have any surficial relations with the detachment further east, and it is difficult to determine if they merge or cross-cut the detachment in the subsurface.

3.3 Subsurface Morphology

Based on the surface geology and structures present in the Silver Peak Range, it is challenging to distinguish if the high-angle faults at the western end of the range are associated with the detachment or if they are associated with the younger deformation that cuts across the

detachment. Borehole data present in the region is used as a key constraint for the subsurface morphology of the basin. Previous gravity surveys conducted in Fish Lake Valley illustrate that the basin is underlain by several gravity lows forming several sub-basins. Utilizing the borehole data and prior gravity surveys as constraints, general attributes of the subsurface can be interpreted, but in order to resolve the subsurface fault geometry a high-resolution relative gravity survey was conducted and 2D forward models were made and tested against the observed gravity.

Surface Geology

The focus of this study is over a west-northwest trending profile that runs from the eastern boundary of the southeastern Volcanic Hills, across the playa, and through the Silver Peak Range (Fig. 3.2). In the southeastern Volcanic Hills, rocks of the Rhyolite Ridge tuff, Argentite Canyon Formation, and the Fish Lake Valley assemblage are exposed (Webber et al., 2017). Rocks of the Fish Lake Valley assemblage overlie the Rhyolite Ridge tuff and are localized along the eastern flank of the Volcanic Hills. Fish Lake Valley assemblage rocks are separated from the Rhyolite Ridge tuff and Argentite Canyon Formation rocks farther west by north-northeast trending series of faults with a down-to-the-east throw. In the playa, a north-northeast striking fault with down-to-the-east throw separates western exposures of Fish Lake Valley assemblage from Quaternary alluvium. About 5 km southeast of the southeastern Volcanic Hills, in the western Silver Peak Range, a curvilinear normal fault with down-to-the-west throw separates Fish Lake Valley assemblage rocks in the footwall from Quaternary alluvial deposits in the playa (Fig. 3.1). The Fish Lake Valley assemblage rocks along the western range front of the Silver Peak Range have no exposed base and consist of at least 300 m

(Oldow et al., 2009) of poorly lithified claystone interbedded with sandstone and siltstone. The assemblage is faulted internally and is separated from older Cenozoic rocks to the east by a north-northeast trending normal fault dipping down to the west (Fig. 3.1). East of this north-northeast trending fault, rocks of the Silver Peak Formation and overlying Rhyolite Ridge tuff are exposed. The Silver Peak Formation is at least 175 m thick and is composed of interbedded fine- to coarse-grained sandstone, conglomeratic sandstone, and argillite that passes upward into interbedded cobble and boulder conglomerate, feldspathic wacke and argillite (Oldow et al., 2009). A small wedge of the Rhyolite Ridge tuff about 75 m thick unconformably overlies the Silver Peak Formation and is mainly composed of moderately indurated nonwelded ash containing lithic clasts and subordinate phenocrysts. A north-northeast striking normal fault that dips down to the west juxtaposes the Rhyolite Ridge tuff wedge next to the Silver Peak Formation in the footwall. East of this north-northeast striking fault, the Silver Peak Formation consists of 20 m of interbedded pebble to boulder conglomerate, argillite, and feldspathic sandstone that passes upward into a middle section of 165 m of interbedded argillite and feldspathic sandstone and an upper 35 m section containing interbedded pebble to cobble conglomerate and feldspathic sandstone. A thin 30 m layer of Rhyolite Ridge tuff overlies interbedded sandstone and conglomerate of the Silver Peak Formation along a sharp angular unconformity. Overlying the Rhyolite Ridge tuff are rocks of the Cave Springs Formation. In the Cave Springs area the thickest section of Cave Springs Formation is exposed and reaches a thickness of at least 300 m (Fig. 3.1). Rocks in this succession consist of a basal ledge of travertine up to 2 m thick that passes upward into thinly interbedded tuffaceous argillite, immature quartzofeldspathic wacke, and conglomerate. The eastern boundary of Cave Springs

Formation is defined by another north-northeast trending fault with a down to the west sense and juxtaposes Cave Springs clastic rocks in the hanging wall next to Rhyolite Ridge rocks in the footwall (Fig. 3.1). This north-northeast striking fault marks the western flank of Rhyolite Ridge (Fig. 3.1). The Rhyolite Ridge tuff exposures in this area are composed of several lithologically distinct facies that reach a total thickness of 350m. The tuff is exposed in a broad northwest-vergent anticline with a shallowly dipping eastern limb and a steeper western limb dipping up to 35° northwest (Oldow et al., 2009). Rocks of the Rhyolite Ridge tuff in the footwall of the syndepositional fault are deformed in a major north-northeast trending anticline and is locally underlain by two faults with reverse motion that have opposing directions of upper plate motion. The western thrust fault is a small displacement, west-directed thrust fault, and in the hanging wall of this fault, there is an east directed thrust fault that is thought to be a reactivated west-dipping normal fault. Several hundred meters to the east of the east directed thrust fault is a northerly striking normal fault with a down-to-the-west throw that is truncated by the detachment further to the north (Fig. 3.1). Along the transect, the eastern extent of Rhyolite Ridge is defined by the northwest directed shallowly dipping detachment fault of Mineral Ridge (Fig. 3.1). In certain locales, alluvial cover obscures the exact location of this contact. The detachment fault structurally separates Paleozoic and Cenozoic rocks of the upper-plate assemblage from the underlying metamorphic tectonites of the lower-plate. The detachment fault is broadly folded about a west-northwest axis and dips about 10-15° to the northwest. About 2.5 km east of the northwest dipping segment of the detachment, the detachment wraps around and is shown to dip to the southeast before resurfacing again with a northwest dip (Fig. 3.1). Within this folded syncline of the detachment, Paleozoic rocks are exposed and in structural contact with the lower-

plate metamorphic tectonites. These Paleozoic rocks reside as klippen on metamorphic rocks and are structurally separated from Cenozoic exposures of the Silver Peak Formation further south by a west-northwest trending longitudinal fault (Fig. 3.1).

Borehole Data

Borehole data provides critical constraints of unit thicknesses for the subsurface geology of the basin. In northern Fish Lake Valley, the geothermal well, EM 17-31 (Hulen et al., 2005) and the oil well, VRS-1 (Garside and Schilling, 1979), both penetrate the detachment fault and into the lower-plate of the pre-Cenozoic basement. The EM 17-31 well is a geothermal exploration well in the Emigrant Peak Geothermal Energy Prospect. It is located about 12 km northwest from the eastern exposed detachment, has a depth of about 890 m, and penetrated the detachment at a depth of 830 m. Although the EM 17-31 well encounters the detachment, it is located about 5 km north of this study's gravity transect and would have to be projected south onto the transect, therefore was not directly used as a constraint in the 2D modeling. Nevada Oil & Minerals geothermal well VRS-1 is located about 18 km northwest of the exposed detachment and penetrates the detachment and lower plate rocks at a depth of 2.6 km. The VRS-1 well was chosen for detailed study because unlike the EM 17-31 well, it is directly aligned with the gravity transect and records thicknesses of the entire Cenozoic section before penetrating the detachment and pre-Cenozoic basement.

In northern Fish Lake Valley, the VRS-1 well is located between the southeastern Volcanic Hills and the western range front of the Silver Peak Range (Fig. 3.2), has a depth of about 2.8 km, and penetrates the detachment and pre-Cenozoic basement at a depth of 2.6 km. Reinterpretation of the VRS-1 lithology and correlation with surficial geologic formations

indicates the following units penetrated by the core. From top to bottom, the geologic units encountered are (Fig. 3.2):

1. Tflv: Plio-Pleistocene Fish Lake Valley assemblage (352 m thick)
2. Trr: Rhyolite Ridge tuff (300 m thick)
3. Tsp: Silver Peak Formation (753 m thick)
4. Tic: Icehouse Canyon assemblage (146 m thick)
5. Pz: Paleozoic rocks (1076 m thick)
6. Mm: metamorphic tectonites (170 m thick to bottom of well)

The depth at which the detachment is encountered in the VRS-1 well is consistent with both 2D end-member structural hypotheses.

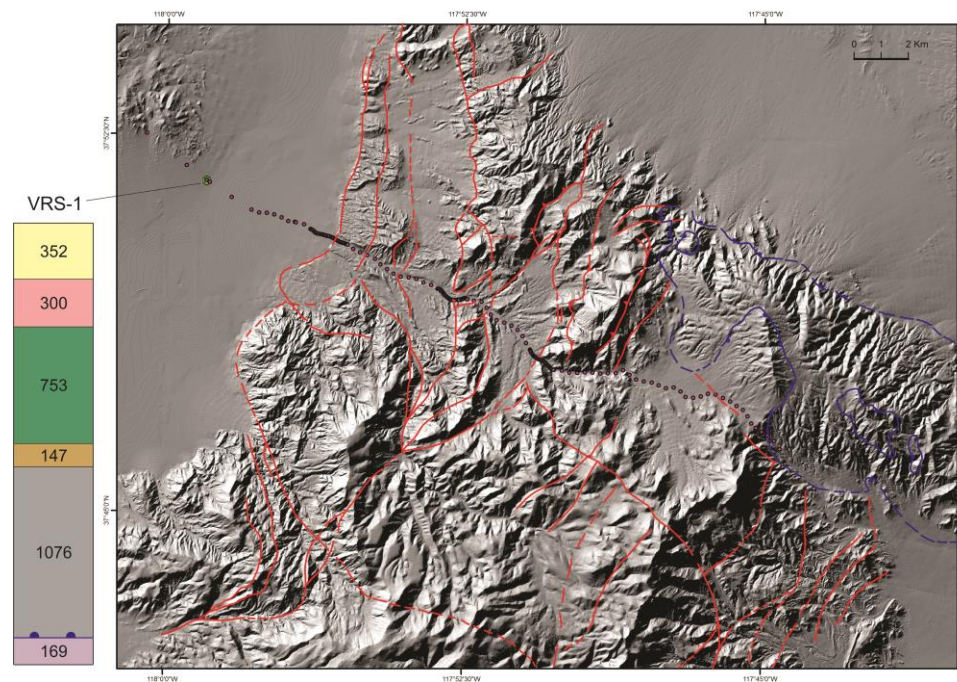


Figure 3.2. Distribution of gravity stations along west-northwest gravity transect in the Silver Peak Range and VRS-1 well location. Location of Nevada Oil & Minerals geothermal well VRS-1 shown by green dot and interpreted stratigraphic section (left; after Garside and Schilling, 1979). Colors indicate formation; see legend in Figure 3.1. High-angle faults are shown in red and detachment faults are shown in blue.

Regional Gravity Field

In previous studies, to gain insight into the subsurface morphology of Fish Lake Valley, a detailed relative gravity survey was conducted and a residual complete Bouguer anomaly (RCBA) was produced then depth inverted to provide estimates of basin geometry and depth (Mueller et al., 2016). Gravity gradients observed in the RCBA (Fig. 3.3) indicate that the eastern limb of northern Fish Lake Valley is underlain by several prominent gravity lows forming several sub-basins with maximum RCBA values ranging from -26 mGal in the northern basin to -28 mGal in the basin just southwest (Mueller et al., 2016). The RCBA was depth inverted in order to provide estimates of depth to basement, and RCBA gravity lows correlate to depths of 2.6 km and 3 km, respectively (Mueller et al., 2016). Based on the resulting depth model, general patterns in the basin can be interpreted, but gravity station spacing is too coarse to accurately determine dips of faults and how the high-angle faults interact with the low-angle detachment in the subsurface. In order to gain a better understanding of the basin geometry and subsurface fault relationships, a high-resolution relative gravity survey was conducted and 2D forward models were constructed to test against the observed gravity.

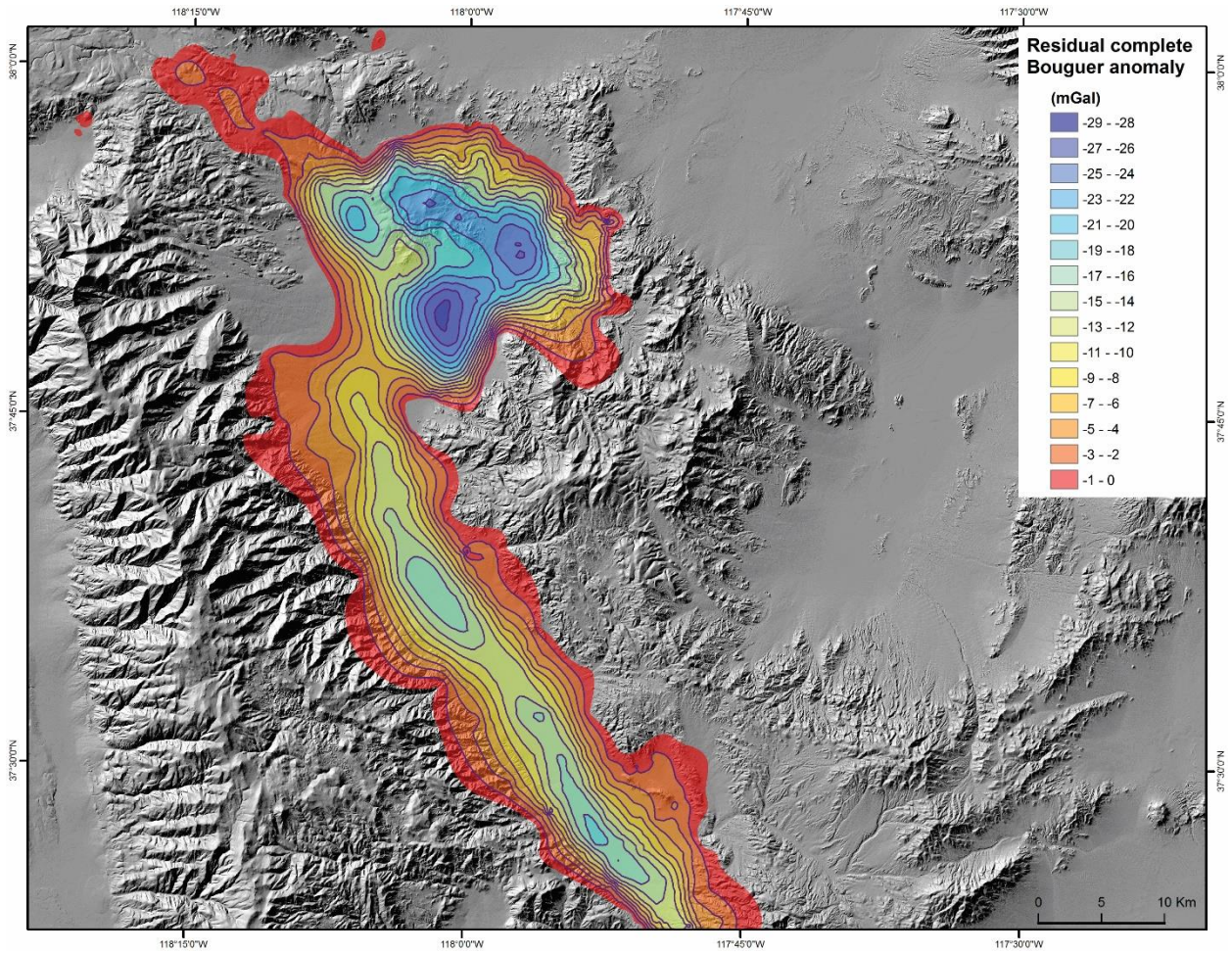


Figure 3.3. Residual complete Bouguer anomaly map of the Fish Lake Valley region. Figure only shows negative values to better illustrate the geometry of basins (Mueller et al., 2016).

CHAPTER 4

GEOPHYSICAL TRANSECT

4.1 Observed Gravity

To understand the subsurface geometry, in the Silver Peak Range and the basin to the west, of the north-northeast striking high-angle faults and their relation to the northwest dipping detachment, a detailed relative gravity survey was conducted and a residual complete Bouguer anomaly (RCBA) was generated. The gravity survey focused on one northwest trending profile through the Silver Peak Range and consisted of about 170 measurements (Fig. 3.2).

The data were collected along a profile using a 4x4 all-terrain vehicle and a Scintrex CG-5 Autograv gravimeter. Two Leica Viva dual frequency global navigation satellite system (GNSS) units were used to determine the positioning of each station. The GNSS positioning was collected using real-time kinematic acquisition, which was able to provide positioning of 2.5 cm or better, and then post-processed using the Leica GeoOffice software. The data were post-processed in an Earth Centered-Earth-Fixed (ECEF) frame by processing base-station data together with Continuously Operating Reference Stations (CORS) using the National Geodetic Survey (NGS) supported website Online Positioning User Service (OPUS). At each station, the relative gravity value was recorded, which consisted of an average of 1 second measurements over a duration of 60 seconds. Three relative gravity values were recorded at each station in order to identify any errors that may have occurred during the occupation. All measurements are referenced to a common base station which was reoccupied at the beginning and end of each field day. A secondary base station, located at the GNSS base station, was also measured twice a day. The gravity base station, located in Dyer, Nevada, was referenced to an absolute gravity

station located at the Tonopah airport 8 miles east of Tonopah, Nevada. The station locations determined by GNSS have a relative uncertainty ranging between 0.016 and 0.011 m. The base station in Dyer, Nevada has a position of Latitude: 37° 52' 4.384698", Longitude: 117° 58' 6.337383" with a maximum uncertainty of 0.016 m (± 0.003), and was used to transform all field observations into the ECEF frame. Along the gravity transect, measurements were taken with a nominal spacing of 300 meters, but when crossing over known high-angle faults, spacing was reduced to 50 meters about 1 km before and after crossing the fault trace. This reduction in spacing of measurements was done in order to acquire a higher resolution of shallow features and more detailed gravity data. This will be able to help determine the location and dips of faults more precisely because direct determination of subsurface fault-dips cannot be resolved with the acquisition spacing of 300 meters.

A complete Bouguer anomaly was computed by combining measurements from our gravity survey with over 72,000 gravity stations, within 180 km of Fish Lake Valley, downloaded from the Pan American Center for Earth Studies (PACES) and over 2,400 measurements collected by previous students from The University of Texas at Dallas (Fig. 4.1). All observed values were reduced in conformity with the standards established by the U.S. Geological Survey (Hildenbrand et al., 2002) and the Standards/Format Working Group of the North American Gravity Database Committee (Hinze et al., 2003) for Bouguer computation using the spreadsheet by Holom and Oldow (2007). All gravity data for our survey are referenced to ellipsoidal heights, which were acquired directly from the GNSS positioning for our stations. In contrast, PACES data are referenced to orthometric heights and were transformed to ellipsoidal using the NGS National Oceanic and Atmospheric Administration

program, Geoid09. The consistency between our measurements and the PACES values was determined by reoccupying 24 pre-existing stations, which yielded a misfit of between -0.45 and 0.95 mGals. Our gravity data were terrain corrected for both the outer and inner terrain correction in MatLab using the GravProc program developed by Dr. John Ferguson at The University of Texas at Dallas. A regional complete Bouguer anomaly was produced using a reduction density of 2.67 g/cm^3 and gridded in Geosoft Oasis Montaj using a minimum curvature technique (Mickus et al., 1991).

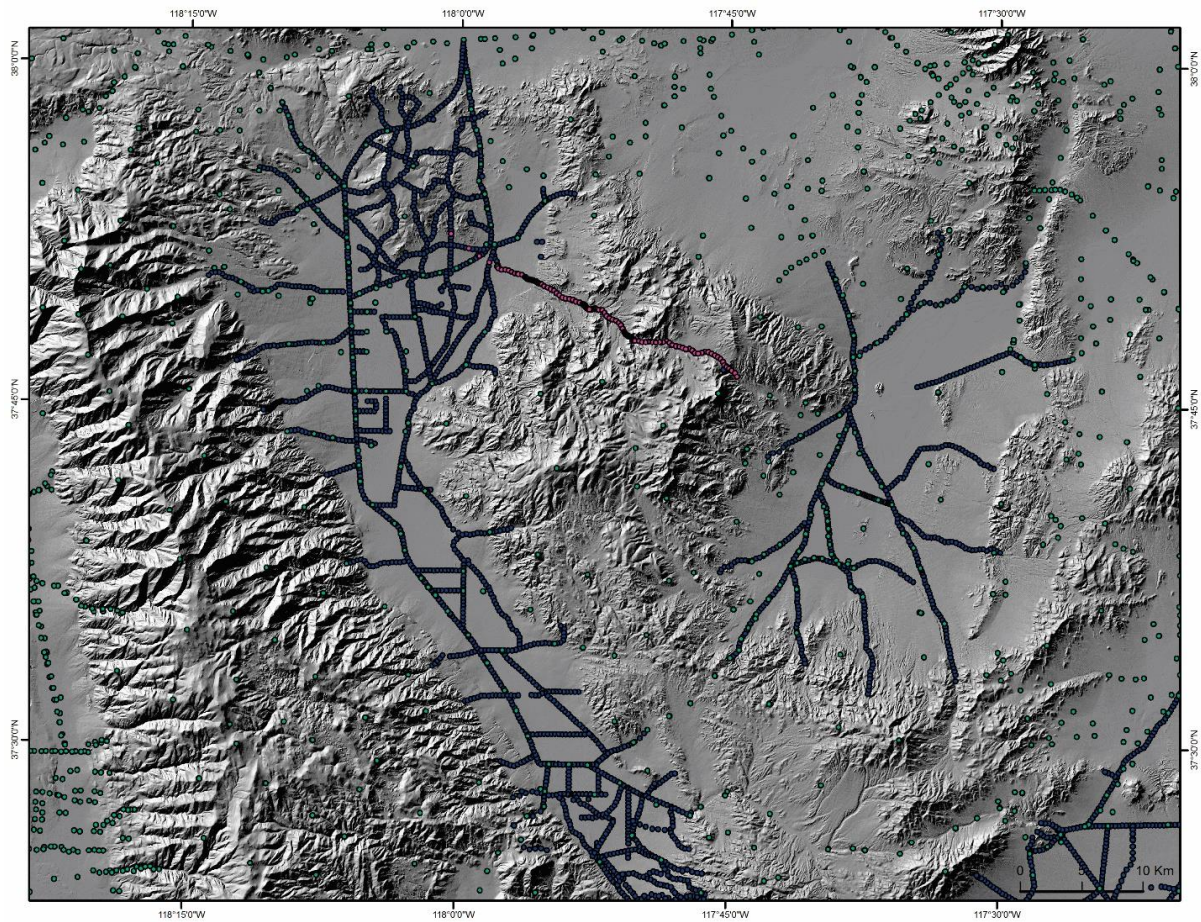


Figure 4.1. Spatial distribution of gravity stations. Stations acquired by The University of Texas at Dallas from summer 2015 for this specific study are shown in pink, other stations taken by The University of Texas at Dallas from summers 2011-2016 are shown in blue, and stations obtained by the Pan American Center for Earth and Environmental Studies are shown in green.

The complete Bouguer anomaly (CBA) for the study region shows a trend from low values on the west to higher values on the east. It is characterized by an increase in the CBA from the southwest to northeast direction from about -232 mGal to -202 mGal, respectively (Fig. 4.2). This trend is characteristic of the whole region and obscures the gravitational signature produced by the shallow-seated sources of interest. In order to interpret these gravity data in terms of basin geometry, the gravitational effects of extraneous geological features, such as the regional trend, must be removed. Once the regional gravity trend is removed from the CBA, a residual complete Bouguer anomaly is produced and is interpreted directly in terms of basin geometry.

The CBA was used to produce a residual complete Bouguer anomaly (RCBA) for the Silver Peak Range. The objective of computing an RCBA is to isolate the gravity signature of the basin by removing the regional gravity field not attributed to the basin of interest. The gravity effect of regional-scale geologic features, such as the Sierra Nevada batholith, is eliminated by fitting a first-order polynomial surface to the regional trend (Fig. 4.3). This surface produces a gradient which represents the application of a very high-pass filter to the data. The gradient is then projected to each station along the gravity transect of interest and subtracted from the complete Bouguer anomaly to effectively remove the regional gravity trend of the Sierra Nevada. The difference between the projected first-order polynomial and the CBA represents a residual anomaly map. The RCBA produced is interpreted to be due solely to local shallow-seated sources and gives better definition of those sources because the interfering regional trend has been removed.

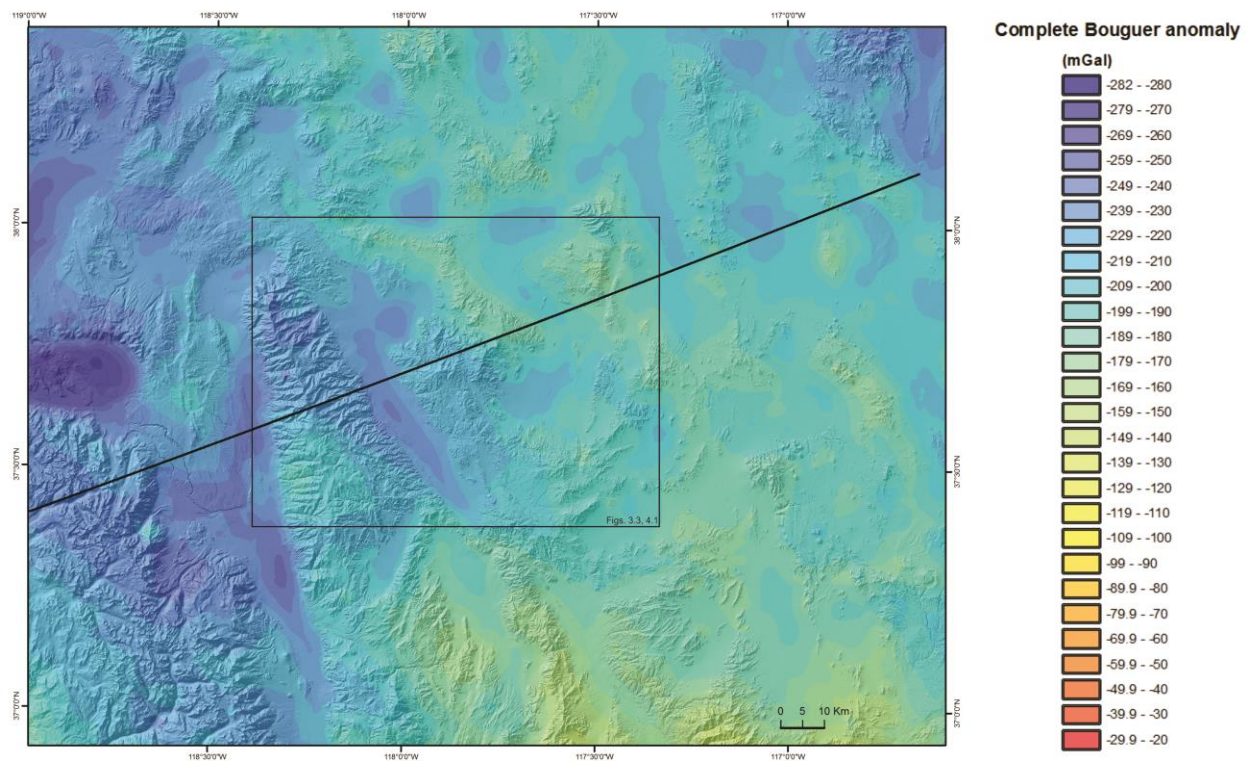


Figure 4.2. Complete Bouguer anomaly of the region. The black line from the SW Sierra Nevada to the NE central Great Basin was used to describe the characteristics of the regional trend. The black box shows the extent of Figures 3.3 and 4.1.

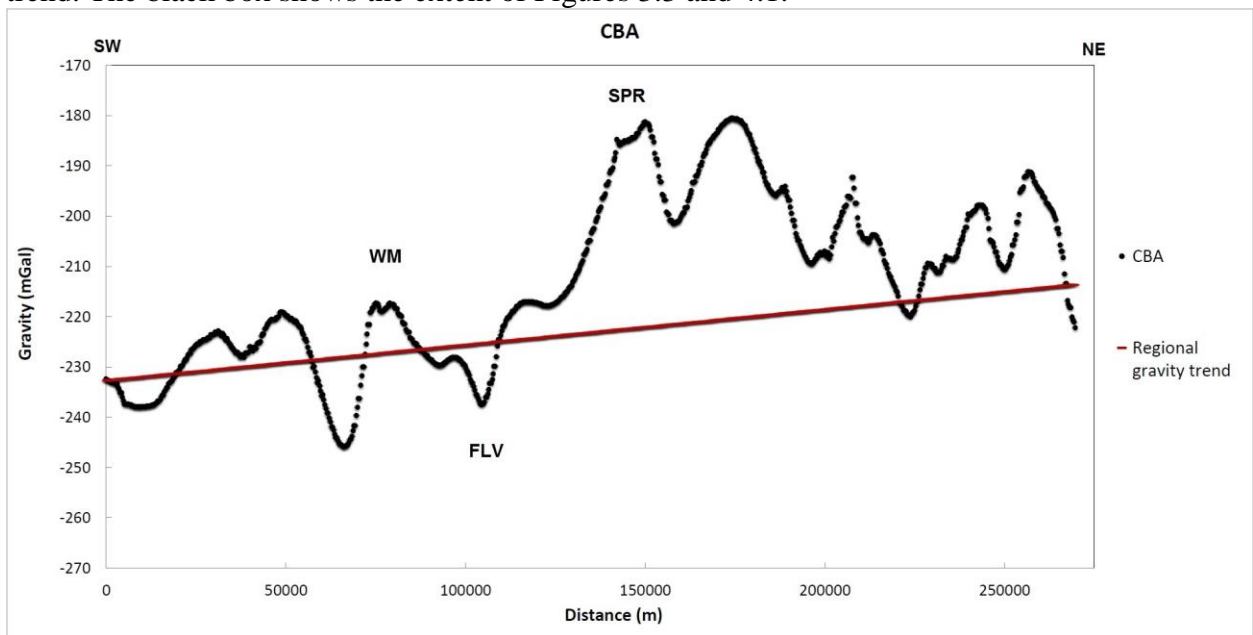


Figure 4.3. First order polynomial of the complete Bouguer anomaly used as a regional trend.

The RCBA (Fig. 4.4) for the Silver Peak Range shows a trend from low values on the northwest in the basin to high values on the southeast in the Silver Peak Range. The northwest area of the transect has a maximum gravity low value of -23 mGals and gradually increases towards the southeast to a maximum high of 7 mGals (Fig. 4.4). The modeled anomaly along the transect reveals important horizontal steps in the RCBA. Starting at the northwest end of the transect, there is a gravity gradient decreasing from -19 mGal to a low of -23 mGal from northwest to southeast (Fig. 4.5). Further to the southeast, the gravity gradient gradually increases from the low of -23 mGal to a high of 2.2 mGal over a distance of about 9 km. Continuing along the transect, there is a gravity gradient decreasing from 2.2 mGal to -1.46 mGal over a distance of 1.6 km before abruptly increasing slightly back up to 0.7 mGal over 0.9 km. The gradient gradually increases from 0.7 mGal to 6.6 mGal along a distance of 4.6 km. Then over a short distance of 0.5 km, there is a slight decrease in gravity to a relative low of 5.1 mGal before it increases back up for about 1 km to a high of 7 mGal. The gravity then starts to decrease from 7 mGal to about 4.5 mGal over the last 3 km of the transect (Fig. 4.5).

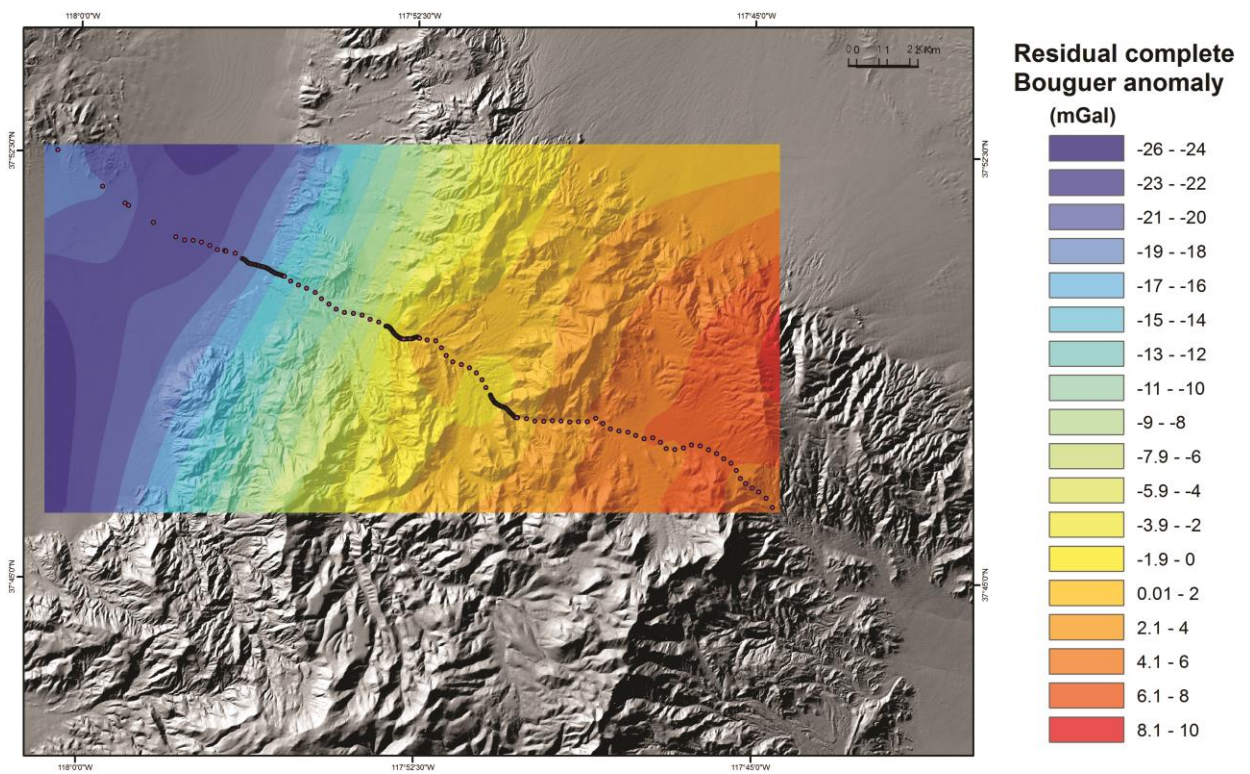


Figure 4.4. Residual complete Bouguer anomaly after removal of the regional trend of the Silver Peak Range.

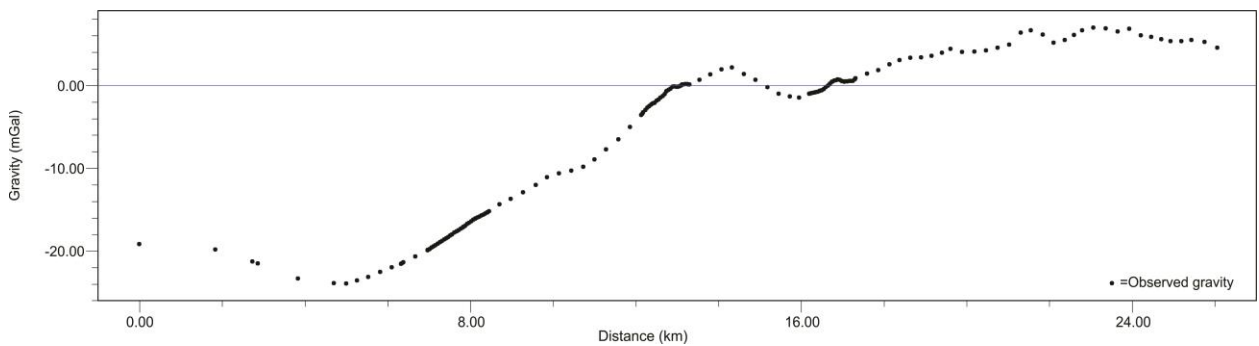


Figure 4.5. Two-dimensional representation of the residual complete Bouguer anomaly. Station locations shown on Figure 4.4.

4.2 Two-Dimensional Forward Models

The subsurface geometry of the Silver Peak Range was further assessed by two-dimensional forward models. The 2D forward model provides constraints on the locations and dips of inferred subsurface faults, and models how the high-angle faults relate to the detachment.

The 2D forward model is based on geologic cross-sections constructed from a synthesis of stratigraphic relations, well data, preserved outcrop relations, and mapped faults. Where misfits in the predicted and observed gravity were recognized, the geologic sections were revised and modified and the gravity signature recomputed iteratively to bring the model in conformity with the observed gravity. Although containing uncertainties, these models incorporate geologic relations from our understanding of the structure and stratigraphy of the study area and help improve our knowledge of the subsurface architecture.

Two end-member structural hypotheses were tested to contrast the modeled gravity anomaly and the residual gravity signal, essentially testing whether a smooth or stepped contact with the basal metamorphic rocks is a better fit. In the first end-member hypothesis, the detachment is modeled as a planar detachment projected to the northwest with an initial dip of about 15° , and all high-angle faults merge into the detachment at depth (Fig. 4.6). In the second end-member model, the cross-cut model (Fig. 4.7), the low-angle detachment is also projected to the northwest with a dip of 15° , but the western high-angle faults cross-cut and offset the detachment. 2D forward modeling of the residual anomaly was carried out using Geosoft GM-SYS modeling software. We located the positions and determined the dips of faults based on inflections in the observed gravity gradients. Constant densities are assigned to each of the

geologic units modeled (Table 1) and were established by best fitting the gravity measured at the VRS-1 borehole, which penetrated the basement (Mueller et al., 2016).

Table 4.1. Geologic units with brief lithologic descriptions and densities used in two-dimensional models.

Unit	Model density (g/cm ³)	Lithology
Qal	1.80	Quaternary alluvial and lacustrine sediments
Tflv	2.20	moderately indurated mudstone, sandstone, and minor conglomerate
Tcs	2.35	interbedded volcanogenic argillite, sandstone, and conglomerate
Trr	2.38	non-welded rhyolite tuff and sandstone interbeds
Tsp	2.45	moderately to well indurated mudstone, sandstone, and conglomerate
Ta	2.60	andesite flows and lahar locally underlain by crystal-rich ashflow tuff
Pz	2.75	Proterozoic and Paleozoic carbonate and siliciclastic rocks
mm	2.80	metamorphic tectonites

In the merging model (Fig. 4.6), the detachment is planar and projected to the northwest with an initial dip of about 15° and all high-angle faults are shown to sole into the detachment. This model currently shows that the detachment is still active during deposition of Fish Lake Valley assemblage. Starting in the northwest end of the transect and moving southeast, there is a gravity gradient decreasing from -19 mGal to -21 mGal. This is represented by two down-to-the-east normal faults both dipping at 80° and soling into the detachment (Fig. 4.6). This fault geometry indicates that the flat projected detachment achieves a maximum depth of about 1650

m under the southeast Volcanic Hills, west of the playa. Continuing southeast there is a small decrease from -21 mGal to a maximum low of -23 mGal. This decrease in gradient is modeled by one down-to-the-east fault with a dip of 75° that soles into the planar detachment at a depth of 1060 m (Fig. 4.6). Just to the west of the normal fault, the VRS-1 well is present and indicates that the detachment was encountered at a depth of 1200 m. Further to the southeast, the gravity gradient gradually increases from the low of -23 mGal to -1 mGal over a distance of 7.7 km. This gradient is modeled by seven down-to-the-west extensional faults with dips that range from 70° in the northwest and progressively decreasing to 45° in the southeast (Fig. 4.6). In the merging model, all faults merge into the detachment and The Fish Lake Valley Assemblage only reaches a maximum thickness of 490 m, with the underlying detachment at a depth of about 900 m (Fig. 4.6). A small gravity gradient increasing from -1 mGal to 2.2 mGal to the southeast is modeled similarly in each end member. It is represented by a 45° dipping, down-to-the-west listric fault that merges into the detachment at a depth of -440 m and does not offset the metamorphic basement. Continuing along the transect, there is a gravity gradient decreasing from 2.2 mGal to -1.46 mGal over a distance of 1.6 km before abruptly increasing slightly back up to 0.7 mGal over 0.9 km. This undulating gradient is modeled by a north-northeast trending anticline that exposes rocks of the Silver Peak Formation, Rhyolite Ridge, and Cave Springs Formation, and is bounded on the east by a north-northeast trending fault that dips to the west at 60° (Fig. 4.6). In this model, the bounding fault is modeled as a listric fault that merges into the detachment at -1100 m depth. Then the gradient gradually increases from 0.7 mGal to 6.6 mGal along a distance of 4.6 km and is modeled by two faults with reverse motion that have opposing directions of upper plate motion. The western most fault is a small-displacement,

west-directed thrust fault, and dips to the east at 45° (Fig. 4.6). In the hanging wall of the west-directed thrust fault, there is a west dipping normal fault that was reactivated and accommodated east-directed reverse motion. Further to the southeast there is a down-to-the-west listric fault that merges with the detachment at a depth of about -1600 m and has a westerly dip of 50° (Fig. 4.6). Reaching the high of 6.6 mGal, this is modeled by the surface exposure of the metamorphic tectonites which was exhumed by a 15° dipping northwest-directed detachment. Then there is a slight decrease in gravity to a relative low of 5.1 mGal before increasing to a high of 7 mGal which is modeled as a thin layer of alluvium sitting on top of the exposed metamorphic basement. The decrease in gravity from 7 mGal to about 4.5 mGal is represented by no more than 150 m of Paleozoic klippen residing on metamorphic tectonites (Fig. 4.6).

In the cross-cut model (Fig. 4.7), the eastern low-angle detachment is projected to the northwest with an initial dip of about 15° , and high-angle faults at the western end of the transect are exhibited to cross-cut and offset the detachment. These western high-angle faults are modeled to be syndepositional with the Fish Lake Valley assemblage. At the northwest end of the transect and moving southeast, the gravity gradient decrease from -19 mGal to -21 mGal is represented by two extensional faults dipping down-to-the-east at 80° . Both faults offset and step the detachment down to the east with offsets of 127 m and 98 m, respectively (Fig. 4.7). Continuing southeast there is a small gradient decrease from -21 mGal to a maximum low of -23 mGal. This gradient is modeled as one down-to-the-east extensional fault with a dip of 75° that cuts the detachment at a depth of 1220 m and offsets it by 322 m (Fig. 4.7). To the west of the normal fault, the VRS-1 well is encountered and indicates that the detachment was encountered at a depth of 1200 m. Continuing to the southeast, the gravity gradient gradually increases over a

distance of 7.7 km from the low of -23 mGal to -1 mGal. This gradient is modeled by seven down-to-the-west extensional faults with dips ranging from 70° in the northwest and progressively decreasing to 45° in the southeast. All seven of these faults offset the detachment westward in a stair-step fashion and have offsets from northwest to southeast of 279 m, 278 m, 167 m, 126 m, 136 m, 115 m, and 72 m, respectively (Fig. 4.7). In this section, the thickness of The Fish Lake Valley Assemblage reaches a maximum of 750 m in the basin with the detachment at a maximum depth of 1540 m (Fig. 4.7). The small gravity gradient increasing from -1 mGal to 2.2 mGal to the southeast is modeled similar to the merging end member hypothesis. It is characterized by a 45° dipping, down-to-the-west listric fault that soles into the detachment at a depth of -500 m and does not offset the metamorphic basement (Fig. 4.7). Continuing southeast, there is a gravity gradient decreasing from 2.2 mGal to -1.46 mGal before abruptly increasing slightly back up to 0.7 mGal over a distance of 2.5 km. Similar to the previous merging model (Fig. 4.6), this undulating gradient is modeled by a north-northeast trending anticline that exposes rocks of the Silver Peak Formation, Rhyolite Ridge, and Cave Springs Formation, and is bounded on the east by a 60° west-dipping north-northeast trending fault. In the cross-cut model, this eastern bounding fault is shown to cross the detachment at a depth of -1175 m and offset it by 212 m (Fig. 4.7). Both models demonstrate that this west dipping fault bifurcates in the subsurface and has encountered two different episodes of activity. Initially the fault was listric and merged into the detachment when accommodating space for syndeposition of the Silver Peak Formation and Rhyolite Ridge tuff, then was reactivated again for deposition of The Cave Springs formation. Then the gradient increases from 0.7 mGal to 6.6 mGal along a distance of 4.6 km and is modeled by two faults with reverse motion that have

opposing directions of upper plate motion (Fig. 4.7). The western most fault is a west directed thrust fault and dips to the east at 45° . In the hanging wall of the west-directed thrust fault, there is a west dipping normal fault that was reactivated and accommodated east-directed reverse motion. Further southeast there is a 50° west dipping listric fault that merges with the detachment at a depth of about -1600 m (Fig. 4.7). The high anomaly of 6.6 mGal is characterized by the surface exposure of the metamorphic tectonites, which was exhumed by a 15° dipping northwest-directed detachment. There is a slight decrease in gravity to a relative low of 5.1 mGal before increasing to a high of 7 mGal that is modeled by a thin layer of alluvium sitting on top of the exposed metamorphic basement (Fig. 4.7). The decrease in gravity from 7 mGal to about 4.5 mGal is represented the same way in both models by no more than 150 m of Paleozoic klippen residing on metamorphic tectonites.

Two different end member models were tested against the observed gravity to help explain subsurface relationships between the high-angle faults and the low-angle detachment. In both models, the low angle detachment is projected to the northwest with an initial dip of about 15° . In the merging model (Fig. 4.6), the projected detachment is planar throughout and all high-angle faults sole into the detachment whereas in the cross-cut model (Fig. 4.7), high-angle faults at the western end of the transect are shown to cross-cut and offset the detachment. For the most part, the southeastern end of the transect (SPR) is represented similarly in both end member hypotheses, and the differences observed between the models are localized at the northwestern end, in northern Fish Lake Valley. The merging model produced a misfit error between the observed and calculated gravity anomaly of 1.216 mGal (Fig. 4.6). The error in this model is localized in the Fish Lake Valley basin at the northwest end of the transect which demonstrates

that if all the high-angle faults sole into the detachment, the calculated gravity anomaly is a few mGals higher than the observed gravity. In contrast, the cross-cut end member hypothesis computed a misfit error between the observed and calculated gravity anomalies of 0.464 mGal (Fig. 4.7), about 1/3 of the net error in the merging model. In this model, the high-angle faults at the northwestern end of the transect offset the detachment in a stair-step manner, and the misfit that was observed in the previous merging model is now eliminated in this model. The high-angle offsets on the detachment provides for more accommodation space of the low density Fish Lake Valley assemblage rocks, which then produces a lower gravity anomaly. Between the two end-member structural hypotheses tested against the observed gravity, results indicate that the superior two-dimensional model is the cross-cut model (Fig. 4.7).

4.3 Displacement Component Determinations

High-angle faults that demonstrate relative vertical offsets with Pliocene to Quaternary activity were evaluated to develop and estimate of displacement transfer related to the current episode of transtensional deformation. For this purpose, a 2D forward model is aligned parallel to the extension direction and provides an estimate of transcurrent displacement along high-angle faults in the Silver Peak Range during west-northwest directed extension since ~5-3 Ma. The vertical component of displacement for all structures was estimated from subsurface offset of the contact between the upper- and lower-plates determined at depth from the 2D section. Using the vertical component of motion together with the dip of each structure from the 2D model, the horizontal extension and net slip for each structure can be derived (Fig. 4.8). This can be computed trigonometrically or geometrically for cross sections oriented parallel to the regional extension direction.

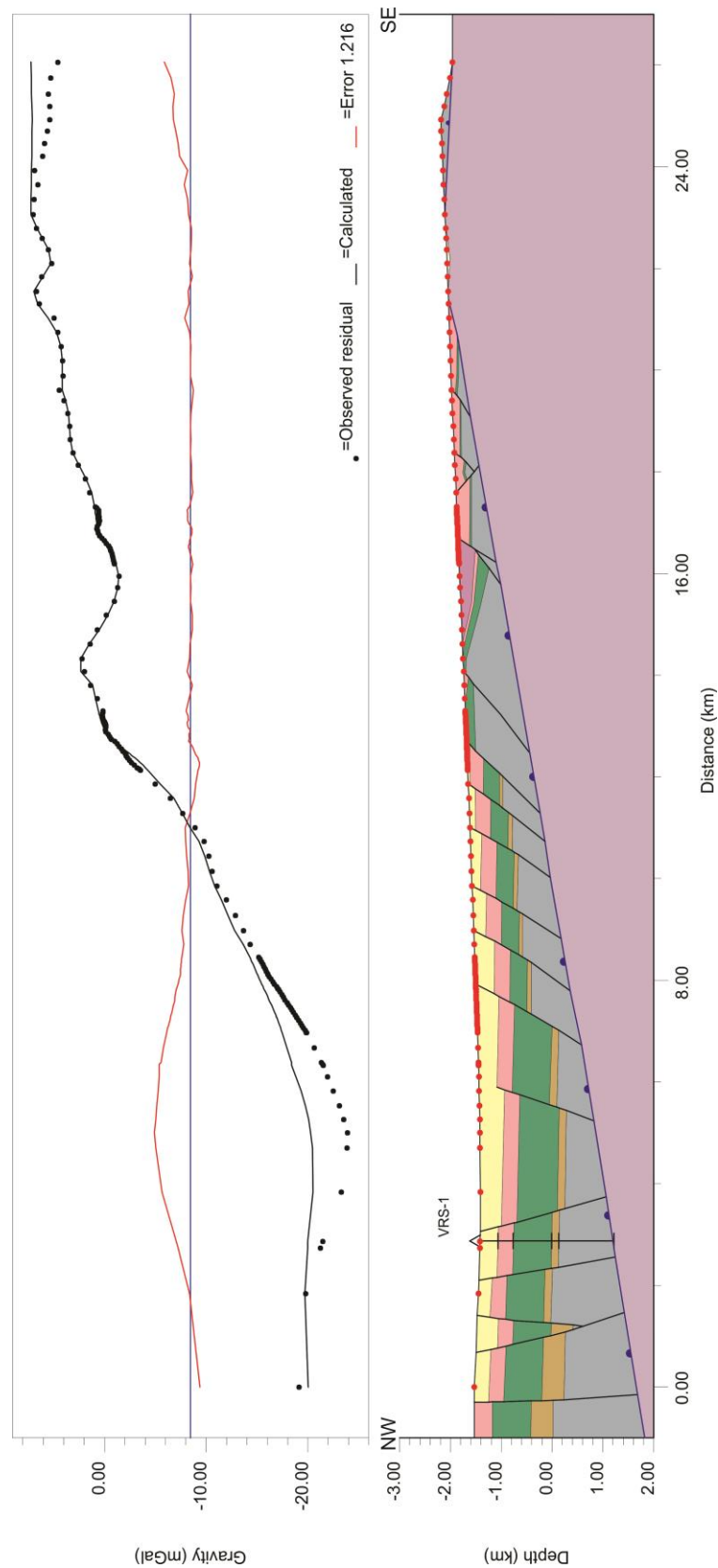


Figure 4.6. Two-dimensional geophysical merging model. Modeled RCBA at field station locations shown by dotted line. Solid black line – forward calculated gravity; red line – error between observed residual and calculated gravity; triangle top – VRS-1 well. Geologic units are incorporated based on their mapped distribution in Figure 3.1. In this end-member model, high-angle faults are modeled to be listric, and merge into the planar low-angle detachment.

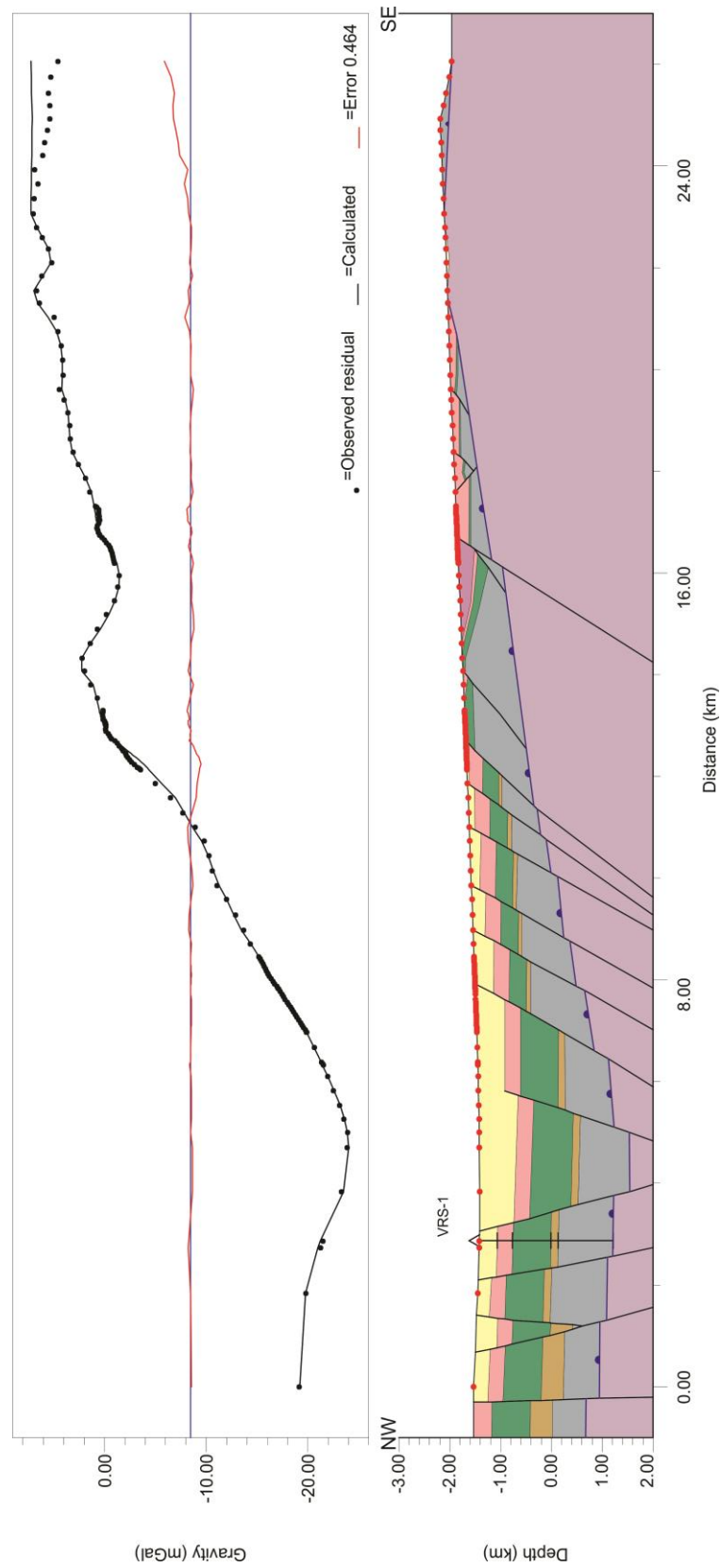


Figure 4.7. Two-dimensional geophysical cross-cut model. Modeled RCBA at field station locations shown by dotted line. Solid black line – forward calculated gravity; red line – error between observed residual and calculated gravity; triangle top – VRS-1 well. Geologic units are incorporated based on their mapped distribution in Figure 3.1. In this end-member model, high-angle faults are modeled to cross-cut and offset the low-angle detachment in the subsurface.

Equation 1:

$$D_{HC} = V/\tan(\Theta)$$

D_{HC} = horizontal component of dip-slip movement

Θ = fault dip angle

V = vertical component of displacement

Once the horizontal component of dip-slip movement is determined, the horizontal extension can be calculated. The horizontal extension can be derived using the value of the dip slip projected to horizontal and the angle between the strike of the fault and the inferred extension direction. In this area, the extension direction is constrained to N65°W and the 2D section is aligned parallel to this direction.

Equation 2:

$$HE = D_{HC}/\sin(\emptyset)$$

HE = horizontal extension

\emptyset = the angle between fault strike and the extension direction.

Now that the horizontal extension has been computed, the net slip can be solved for. The net slip of each structure was calculated by using the vertical offset and the computed horizontal extension, making the assumption that all slip is parallel to the extension direction.

Equation 3:

$$NS = \sqrt{V^2 + HE^2}$$

The 2D modeling results show that from the eastern southeastern Volcanic Hills moving southeast, the decrease in the gravity gradient from -19 mGal to a low of -23 mGal is modeled by three down-to-the east extensional faults with a total vertical displacement on the detachment of

about 550 m (Fig. 4.7). Continuing along the transect, a gradient from -23 mGal to the maximum of 7 mGal is modeled with a total of eight down-to-the-west normal faults that cross-cut both the upper- and lower- plate assemblages, and have a summed vertical offset of 1400 m. The calculated cumulative net slip on all structures that offset the low-angle detachment is about 2200 m and with fault dips ranging from 45° to 80° yields a total horizontal extension of 920 m.

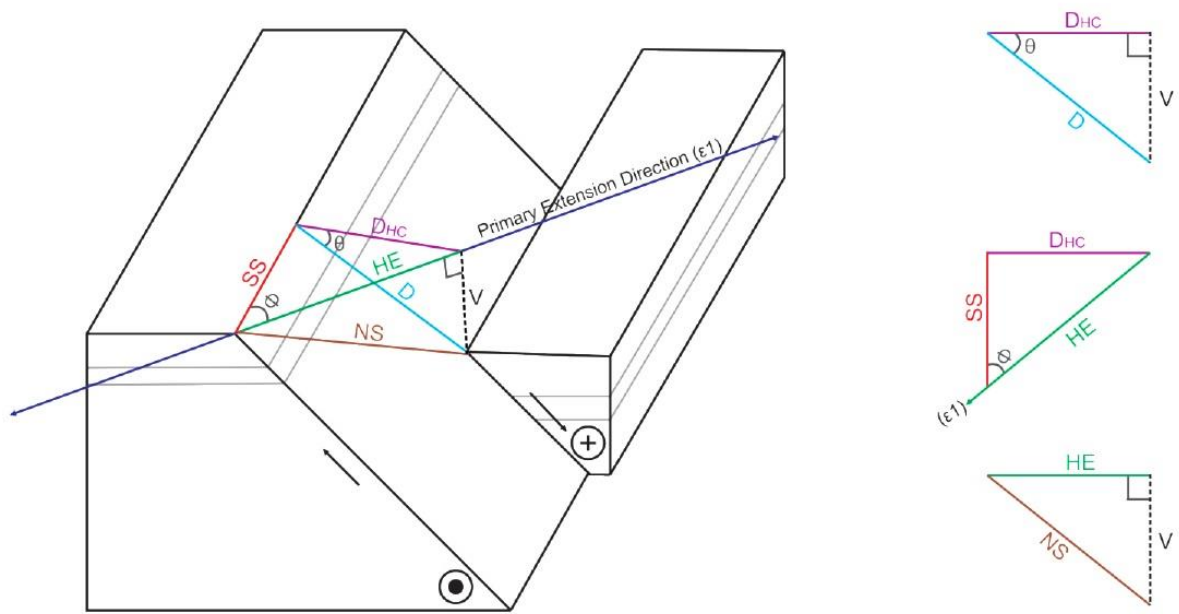


Figure 4.8. Fault displacement components. Block and trigonometric diagrams used in the derivation of fault displacement components. Components: D_{HC} – horizontal component of dip slip movement, SS – strike slip component, HE – horizontal extension, NS – net slip, V – vertical offset, D – dip slip component, Θ – true dip of the fault, \emptyset – acute angle between strike and inferred extension direction. Modified from Biholar, 2011.

CHAPTER 5

DISCUSSIONS AND CONCLUSIONS

Based on surficial relations in the Silver Peak Range, it is difficult to differentiate which high-angle faults are associated with the detachment and which faults are associated with the younger deformation that cuts across the detachment. To improve our knowledge of the subsurface geometry, two different possible 2D end member models were tested against the observed gravity. In the merging model, all high-angle faults were modeled to sole into the detachment in the subsurface (Fig. 4.6). This model produced a misfit error between the observed and calculated gravity anomaly of 1.216 mGal. The misfit in this model is localized at the northwest end in the Fish Lake Valley basin. This model demonstrates that if all the high-angle faults sole into the detachment the calculated gravity anomaly in the Fish Lake Valley basin is a few mGals higher than the observed gravity. In the cross-cut model, high-angle faults were modeled to cut and offset the detachment in the subsurface (Fig. 4.7). In this model the misfit error between the observed and calculated gravity anomalies is 0.464 mGal. In this model, the high-angle faults at the western end of the transect offset the detachment in a stair-step fashion, and the misfit that was observed in the Fish Lake Valley basin from the previous merging model is now eliminated in this model. The stair-step offset provides for more accommodation space of the low density rocks of the Fish Lake Valley assemblage, which results in a lower gravity anomaly and an overall better fit model. Of the two end member hypotheses tested against the observed gravity, results indicate that the superior two-dimensional forward model is the cross-cut model (Fig. 4.7). Along with the two end member models, hybrid models were also tested along with 2.5 D modeling, but these models showed no significant differences in the calculated anomalies. In the

better-fit cross-cut model, two-dimensional forward modeling results indicate that eight down-to-the west extensional faults in the Silver Peak Range and northern Fish Lake Valley cross-cut both upper- and lower- plate rocks of the SPLM. These faults are related to the current episode of transtensional deformation, which initiated at ~4 Ma, offset the detachment in a stair-step fashion, and help to transfer displacement from the northern ECSZ into the CWL.

Cumulative displacement on the array of high-angle faults of the Silver Peak Range is moderate and provides an estimate of magnitude of displacement transferred from the ECSZ to the CWL since the late Pliocene. The net vertical displacement accumulated on Silver Peak Range Quaternary high-angle faults is 2.221 km, and gives a net slip for the system of 2.181 to 2.452 km. The horizontal component of displacement on the fault array is 0.917 km. Our analysis provides an important constraint on the displacement budget for part of the network of faults underlying the southern Walker Lane.

REFERENCES

- Albers, J.P., and Stewart, J.H., 1972, Geology and Mineral Deposits of Esmeralda County, Nevada: Nevada Bureau of Mines and Geology Bulletin 78, 88 p.
- Argus, D.F., and Gordon, R.G., 1991, Current Sierra Nevada-North America motion from very long baseline interferometry: Implications for the kinematics of the western United States: *Geology*, v. 19, p. 1085-1088.
- Bennett, R.A., Davis, J.L., and Wernicke, B.P., 1999, Present-day pattern of Cordilleran deformation in the western United States: *Geology*, v. 27, p. 371-374.
- Bennett, R.A., Wernicke, B.P., Niemi, N.A., Friedrich, A.M., and Davis, J.L., 2003, Contemporary strain rates in the northern Basin and Range province from GPS data: *Tectonics*, v. 22, p. 3-1 - 3-31.
- Biholar, A.K.C., Late Neogene slip transfer and extension within the curved Whisky Flat fault system central Walker Lane, west-central Nevada [M.S. thesis]: The University of Texas at Dallas, 58 p.
- Coney, P.J., 1979, Tertiary evolution of Cordilleran metamorphic core complexes, in Armentrout, J.M., Cole, M.R., and Terbest, H., Jr., eds., *Cenozoic paleogeography of western United States: Society of Economic Paleontologists and Mineralogists, Pacific Section, Pacific Coast Paleogeography Symposium 3*, p. 15-28.
- Coney, P.J., 1980, Cordilleran metamorphic core complexes: An overview, *in* Crittenden, M.D., Coney, P.J., and Davis, G.H., eds., *Cordilleran metamorphic core complexes: Geological Society of America Memoir 153*, p. 7-34.
- Coney, P.J., and Harms, T.A., 1984, Cordilleran metamorphic core complexes: Cenozoic extensional relics of Mesozoic compression: *Geology*, w. 12, p. 550-554.
- Davis, G.H., and Coney, P.J., 1979, Geologic development of the Cordilleran metamorphic core complexes: *Geology*, v. 7, p. 120-124.
- Diamond, D.S., and Ingersoll, R.A., 2002, Structural and sedimentologic evolution of a Miocene supradetachment basin, Silver Peak Range and adjacent areas, west-central Nevada: *International Geology Review*, v. 44, p. 588-623.
- Dixon, T.H., Miller, M., Farina, F., Wang, H., and Johnson, D., 2000, Present day motion of the Sierra Nevada block and some tectonic implications for the Basin and Range Province, North American Cordillera: *Tectonics*, v. 19, p. 1-24.

- Evernden, J.F., and James, G.T., 1964, Potassium-argon dates and the Tertiary floras of North America: *American Journal of Science*, v. 262, p. 945-974.
- Evernden, J.F., Savage, D.E., Curtis, G.H., and James, G.T., 1964, Potassium-argon dates and the Cenozoic mammalian chronology of North America: *American Journal of Science*, v. 262, p. 145-198.
- Faulds, J.E., and Varga, R.J., 1998, The role of accommodation zones and transfer zones in the regional segmentation of extended terranes: *Geological Society of America Special Paper* 323, p. 1-45.
- Gans, P.B., Mahood, G. and Schermer, E., 1989, Synextensional magmatism in the Basin and Range Province; A case study from the eastern Great Basin: *Geological Society of America Special Paper* 233, p. 1-53.
- Garside, Larry J. and John H. Schilling, 1979, Thermal Waters of Nevada, *Bulletin* 91, Nevada Bureau of Mines and Geology.
- Geosoft Inc., 2011, GM-SYS Profile Modeling, Gravity and Magnetic Modeling Software for Oasis Montaj, Version 7.3, Geosoft Inc., Toronto, ON, Canada.
- Hardyman, R.F., and Oldow, J.S., 1991, Tertiary tectonic framework and Cenozoic history of the central Walker Lane, Nevada, in Raines, G.L., Lisle, R.E., Schafer, R.W., and Wilkinson, W.H., eds., *Geology and Ore Deposits of the Great Basin: Reno, Nevada Geological Society of Nevada, Symposium Proceedings*, p. 279-301.
- Henry, C.D., and Perkins, M.E., 2001, Sierra Nevada-Basin and Range transition near Reno, Nevada: Two-stage development at 12 and 3 Ma: *Geology*, v. 29, p. 719-722.
- Hildenbrand, T.G., Briesacher, A., Flanagan, G., Hinze, W.J., Hittelman, A.M., Keller, G.R., Kucks, R.P., Plouff, D., Roest, W., Seeley, J., Smith, D.A., and Webring, M., 2002, Rationale and Operational Plan to Upgrade the U.S. Gravity Database: U.S. Geological Survey Open-File Report 02-463, 12 p.
- Hinze, W.J., 2003, Bouguer reduction density, why 2.67?: *Geophysics*, v. 68, p. 1559-1560.
- Holom, D.I., and Oldow, J.S., 2007, Gravity reduction spreadsheet to calculate the Bouguer anomaly using standardized methods and constants: *Geosphere* 3, p. 86-90.
- Hulen, J. B., Nash, G. D., and Deymonaz, J., 2005, Geology of the Emigrant Geothermal Prospect, Esmeralda County, Nevada, *Geothermal Resources Council Transactions*, 29, p. 369-380.

- Kerstetter, S.R., Oldow, J.S., and Katopody, D.T., 2016, Mid-Miocene synextensional deposition during north-south extension in a west-northwest trending half-graben in the western Great Basin: Geological Society of America Abstracts with Programs, v. 48, no. 4, doi: 10.1130/abs/2016CD-274463.
- Kirsch, S.A., 1971, Chaos structure and turtleback dome, Mineral Ridge, Esmeralda County, Nevada: Geological Society of America Bulletin, 82, p. 3169-3176.
- Lee, J., Stockli, D., Schroeder, J., Tincher, C., Bradley, D., and Owen, L., 2003, Fault slip transfer in the Eastern California shear zone and Walker Lane, *in* Lee, J., Stockli, D., Henry, C., and Dixon, T., conveners, Penrose Conference: Kinematics and Geodynamics of Intraplate Dextral Shear in Eastern California and Western Nevada: Boulder, Colorado, Geological Society of America, 45 p.
- Mancktelow, N.S., and Pavlis, T.L., 1994, Fold-fault relationships in low-angle detachment systems: Tectonics, v. 13, p. 668-685.
- Mickus, K.C., C.L.V. Aiken, and W.D. Kennedy, 1991, Regional-residual gravity anomaly separation using the minimum-curvature technique: Geophysics, v. 56, no. 2, p. 279-283.
- Miller, M.M., Johnson, D.J., Dixon, T.H., and Dokka, R.K., 2001, Refined kinematics of the Eastern California shear zone from GPS observations, 1993-1998: Journal of Geophysical Research, v. 106. no. B2, p. 2245-2263.
- Mueller, N.J., Kerstetter, S.R., Katopody, D.T., and Oldow, J.S., 2016, Subsurface constraints on late Cenozoic basin geometry in northern Fish Lake Valley and displacement transfer along the northern Fish Lake Valley fault zone, western Nevada: AGU Fall Meeting Abstracts, T41E-2975.
- Oldow, J.S., 1984, Spatial variability in the structure of the Roberts Mountain allochthon, western Nevada: Geological Society of America Bulletin, v. 95, p. 174-185.
- Oldow, J.S., Bally, A.W., Ave Lallemand, H.G., and Leeman, W.P., 1989, Phanerozoic evolution of the North American Cordillera; United States and Canada, *in* Bally, A.W., and Palmer, A.R., eds., The Geology of North America – An Overview: Boulder, Colorado, Geological Society of America, The Geology of North America, v. A, p. 139-232.
- Oldow, J.S., 1992, Late Cenozoic displacement partitioning in the northwestern Great Basin, in Craig, S.D., ed., Structure, Tectonics, and Mineralization of the Walker Lane; Reno, Geological Society of Nevada, p. 17-52.
- Oldow, J.S., Kohler, G., and Donelick, R.A., 1994, Late Cenozoic extensional transfer in the Walker Lane strike-slip belt, Nevada: Geology, v. 22, p. 637-640.

- Oldow, J.S., Aiken, C.L.V., Hare, J.L., Ferguson, J. F., and Hardyman, R.F., 2001, Active displacement transfer and differential block motion within the central Walker Lane, western Great Basin: *Geology*, v. 29, p. 19-22.
- Oldow, J.S., 2003, Active transtensional boundary zone between the western Great Basin and Sierra Nevada block, western U.S. Cordillera: *Geological Society of America, Geology*, v. 31, no. 12, p. 1033-1036.
- Oldow, J.S., Geissman, and J.W., Stockli, D.F., 2008, Evolution and Strain Reorganization within Late Neogene Structural Stepovers Linking the Central Walker Lane and Northern Eastern California Shear Zone, Western Great Basin: *International Geology Review*, v. 50, p. 270-290.
- Oldow, J.S., Elias, E.A., Ferranti, L., McClelland, W.C., and McIntosh, W.C., 2009, Late Miocene to Pliocene synextensional deposition in fault-bounded basins within the upper plate of the western Silver Peak-Lone Mountain extensional complex, west-central Nevada: *Geological Society of America Special Paper 447: Late Cenozoic Structure and Evolution of the Great Basin-Sierra Nevada Transition*, p. 275-312.
- Oldow, J.S., Payne, J.D., Prestia, V.I., McClelland, W.C., and Ferranti, L., 2003, Stratigraphic and Structural Evolution of the Silver Peak Extensional Complex, Western Great Basin, U.S.A., in *Regional Geology and Gold Deposits of the Silver Peak Area, Mineralization Hosted by Metamorphic Core Complexes: Geological Society of Nevada Special Publication 38*, p. 51-78.
- Pan-American Center for Earth and Environmental Studies (PACES), 2005, The University of Texas at El Paso, Gravity database of the United States: <http://www.research.utep.edu>
- Petronis, M.S, Geissman, J.W., Oldow, J.S., and McIntosh, W.C., 2002, Paleomagnetic and $^{40}\text{Ar}/^{39}\text{Ar}$ geochronologic data bearing on the structural evolution of the Silver Peak extensional complex, west-central Nevada: *Geological Society of America Bulletin*, v. 114, p. 1108-1130.
- Petronis, M.S, Geissman, J.W., Oldow, J.S., and McIntosh, W.C., 2007, Tectonism of the southern Silver Peak Range: Paleomagnetic and geochronologic data bearing on the Neogene development of a regional extensional complex, central Walker Lane, Nevada: *Geological Society of America Special Paper 434*, p. 81-106, doi: 10.1130/2007.2434(05).
- Petronis, M.S, Geissman, J.W., Oldow, J.S., and McIntosh, W.C., 2009, Late Miocene to Pliocene vertical-axis rotation attending development of the Silver Peak-Lone Mountain displacement transfer zone, west-central Nevada: *Geological Society of America Special Paper 447: Late Cenozoic Structure and Evolution of the Great Basin-Sierra Nevada Transition*, p. 215-253.

- Reheis, M.C., and Sawyer, T.L., 1997, Late Cenozoic history and slip rates of the Fish Lake Valley, Emigrant Peak, and Deep Springs fault zones, Nevada and California: Geological Society of America Bulletin, v. 109, p. 280-299.
- Robinson, P.T., Mckee, E.H., and Moiola, R.J., 1968, Cenozoic volcanism and sedimentation, Silver Peak region, western Nevada and adjacent California, *in* Coats, R.R., Hay, R.L., and Anderson, C.A., eds., Studies in Volcanology; A Memoir in Honor of Howel Williams: Geological Society of America Memoir 116, p. 577-612.
- Robinson, P.T., Stewart, J.H., Moiola, R.J., and Albers, J.P., 1976, Geologic Map of the Rhyolite Ridge Quadrangle, Esmeralda County, Nevada: U.S. Geological Survey Map GQ- 1325, scale 1:62,500.
- Stewart, J.H., and Poole, F.G., 1974, Lower Paleozoic and uppermost Precambrian Cordilleran miogeocline, Great Basin, western United States, *in* Dickinson, W.R., ed., Tectonics and Sedimentation: Society of Economic Paleontologists and Mineralogists Special Publication 22, p. 28-57.
- Stewart, J.H., and Diamond, D.S., 1990, Changing patterns of extensional tectonics; overprinting of the basin of the middle and upper Miocene Esmeralda Formation in western Nevada by younger structural basins, *in* Wernicke, B.P., ed., Basin and Range extensional tectonics near the latitude of Las Vegas, Nevada: Geological Society of America Memoir 176, p. 447-475.
- Stockli, D.F., Dumitru, T.A., McWilliams, M.O., and Farley, K.A., 2003, Cenozoic tectonic evolution of the White Mountains, California and Nevada: Geological Society of America Bulletin, v. 115, p. 788-816.
- Thatcher, W., Foulger, G.R., Julian, B.R., Svarc, J., Quilty, E., Bawden, G.W., 1999, Present-day deformation across the Basin and Range province, western United States: Science, v. 283, p. 1714-1718.
- Unruh, J., J. Humphrey, and A. Barron, 2003, Transtensional model for the Sierra Nevada frontal fault system, eastern California: Geology, v. 31, no. 4, p. 327-330
- Walker, J.D., Bidgoli, T.S., Didericksen, B.D., Stockli, D.F., and Andrew, J.E., 2014, Middle Miocene to recent exhumation of the Slate Range, eastern California, and implications for the timing of extension and the transition to transtension: Geosphere, v. 10, p. 276-291.
- Webber, A., Oldow J.S., 2017, Two periods of Miocene to contemporary flattening strain during displacement on a low-angle detachment and superposed high-angle faults, Volcanic Hills, southwest Nevada: Geological Society of America Abstracts with Programs, v. 49, no. 6, doi: 10.1130/abs/2017AM-302487.

BIOGRAPHICAL SKETCH

Melissa Ng was born in Dallas, Texas. In 2015, she obtained a bachelor's degree in Geosciences from The University of Texas at Dallas. Melissa began her graduate studies in the Geosciences department at The University of Texas at Dallas in 2015 under the supervision of Dr. John S. Oldow.

CURRICULUM VITAE

Melissa Ng

800 W Campbell Rd, Richardson TX, 75080
University of Texas at Dallas, Department of Geosciences, ROC 21

Education

Master of Science (M.S.) in Geosciences
The University of Texas at Dallas
Summer 2015 – Fall 2018
GPA: 3.78

Bachelor of Science (B.S.) in Geosciences
The University of Texas at Dallas
Fall 2012 – Spring 2015
GPA: 3.12

Research and Experience

Graduate Teaching Assistant, UT Dallas, Dept. of Geosciences
Summer 2016

Graduate Research Assistant, UT Dallas, Dept. of Geosciences
Summer 2015

Undergraduate Field Research Assistant, UT Dallas, Dept. of Geosciences
Summer 2014: Fish Lake Valley, NV

Abstracts

Ng, M., Oldow, J.S., 2017, Geometry of superposed low-angle detachment and high-angle faults in the western Silver Peak Range and northern Fish Lake Valley, Nevada: Geological Society of America Abstracts with Programs, v. 49, no. 6, doi: 10.1130/abs/2017AM-306721.